Comparisons of bispectral and polarimetric cloud microphysical retrievals using LES-Satellite retrieval simulator

Daniel J. Miller[1], Zhibo Zhang[1,2], Steven Platnick[3], Andrew S. Ackerman[4], Frank Werner[2], Celine Cornet[5], Kirk Knobelspiesse[3]

[1]Physics, UMBC, Baltimore, 21250, USA
[2]Joint Center for Earth Systems Technology, UMBC, Baltimore, MD, USA
[3]NASA Goddard Space Flight Center, Greenbelt, MD, USA
[4]NASA Goddard Institute for Space Studies, New York, NY, USA
10 [5]Laboratoire d'Optique Atmosphérique, Université des Sciences et Technologies de Lille, Villeneuve d'Ascq, France

Correspondence to: Daniel J. Miller (DJ-Miller@umbc.edu)

Abstract. Many passive remote sensing techniques have been developed to retrieve cloud microphysical properties from satellite-based sensors, with the most common approaches being the bispectral and polarimetric techniques. These two vastly different retrieval techniques have been implemented for a variety of polar-orbiting and geostationary satellite platforms,

15 providing global climatological datasets. Prior instrument comparison studies have shown that there are systematic differences between the droplet size retrieval products (effective radius) of bispectral (e.g. MODIS, Moderate Resolution Imaging Spectroradiometer) and polarimetric (e.g. POLDER, Polarization and Directionality of Earth's Reflectances) instruments. However, intercomparisons of airborne bispectral and polarimetric instruments have yielded results that do not appear to be systematically biased relative to one another. Diagnosing this discrepancy is complicated, because it is often

20 difficult for instrument intercomparison studies to isolate differences between retrieval technique sensitivities and specific instrumental differences such as calibration, atmospheric correction, etc. In addition to these technical differences the polarimetric retrieval is also sensitive to the dispersion of the droplet size distribution (effective variance), which could influence the interpretation of the droplet size retrieval. To avoid these instrument-dependent complications, this study makes use of a cloud remote sensing retrieval simulator. Created by coupling a large eddy simulation (LES) cloud model

25 with radiative transfer models, the simulator serves as a test bed for understanding differences between bispectral and polarimetric retrievals. With the help of this simulator we can not only compare the two techniques to one another (retrieval intercomparison), but also validate retrievals directly against the LES cloud properties. Using the satellite retrieval simulator we are able to verify that at high spatial resolution (50 m) the bispectral and polarimetric retrievals are indeed highly correlated with one another. The small differences at high spatial resolution can be attributed to different sensitivity

30 limitations of the two retrievals. In contrast, a systematic difference between the two retrievals emerges at coarser resolution. This bias largely stems from differences related to sensitivity of the two retrievals to unresolved inhomogeneities in effective variance and optical thickness. The influence of coarse angular resolution is found to increase uncertainty in the polarimetric retrieval, but generally maintains a constant mean value.

1 Introduction

The cloud droplet size distribution (DSD) is an important microphysical property of liquid-phase clouds. Given the cloud water content, it largely determines the shortwave radiative effects of clouds (Twomey, 1977). It also plays a critical role in cloud-precipitation processes (Pruppacher and Klett, 1978). As a result, anthropogenic perturbation to the DSD could

5 lead to a variety of cloud property changes with significant climate implications (Lohmann et al., 2007).

Many satellite-based techniques have been developed to retrieve cloud DSD properties from regional to global scales. These techniques typically infer DSD properties based on an assumed size distribution shape, characterized by an effective radius (r_e), and an effective variance (v_e). One such retrieval method is called the bispectral total reflectance technique, hereafter referred to as the "bispectral technique," simultaneously retrieves cloud optical thickness (τ) and r_e from a pair of cloud

10 reflectances, one in the visible to near infrared (VNIR) and the other in the shortwave infrared (SWIR) spectral range (Nakajima and King, 1990b). This retrieval technique has been implemented for numerous satellite and airborne instruments, such as the Moderate Resolution Imaging Spectro-radiometer (MODIS, (King et al., 2003; Platnick et al., 2003; 2016)), the Spinning Enhanced Visible and Infrared Imager (SEVIRI, (Roebeling et al., 2006)), and the National Polar-orbiting Partnership Visible Infrared Imaging Radiometer Suite (NPP VIIRS, (Rosenfeld et al., 2014)).

15 A second, vastly different, retrieval technique is the multi-angular polarimetric reflectance technique, hereafter referred to as the "polarimetric technique". This retrieval requires multi-angular observations of the polarized reflectance in the cloudbow scattering region. In addition to r_e, the polarimetric technique can also retrieve v_e (Bréon and Goloub, 1998). Global retrievals using the polarimetric technique were first demonstrated by the Polarization and Directionality of Earth Reflectance (POLDER, (Deschamps et al., 1994)) instruments operating from 1996 to 2013 on three different satellite

20 platforms. The Aerosol Polarimetry Sensor (APS, (Mishchenko et al., 2007)) would have been the first space-borne multi-angular polarimeter from U.S. to provide global aerosol and cloud property retrievals. Unfortunately, it was lost as a result of the satellite launch failure in 2011, which suddenly interrupted development of polarimetric-based remote sensing in the U.S. Recognizing the great potential of polarimetric techniques for aerosol and cloud remote sensing, NASA has invested heavily in recent years on the development of airborne polarimeters, such as the Research Scanning Polarimeter (RSP, (Cairns et al.,

25 1999)), the Airborne Multi-angle Spectro-Polarimetric Imager (AirMSPI, (Diner et al., 2013)) and the Airborne Hyper-Angular Rainbow Polarimeter (Air-HARP, (Martins et al., 2017)). Moreover, several space-borne missions are in development, such as the Multi-Angle Imager for Aerosols (MAIA, (Liu and Diner, 2017)), HARP, the Plankton, Aerosols, Cloud, ocean Ecosystem mission (PACE) and the Multi-viewing, Multi-channel, Multi-polarization imaging mission (3MI, (Marbach et al., 2013)). Each of these missions will have a multi-angular polarimeter on-board. In the foreseeable future, we

30 may expect to have operational global retrievals of cloud droplet size distributions from both bispectral and polarimetric methods.

Because bispectral and polarimetric remote sensing techniques are the primary tools we have to obtain DSD observations on a global scale, it is important to identify and explain the differences between them so we can better understand the

advantages and limitations of each technique. A satellite retrieval intercomparison of POLDER and MODIS r_e retrievals by Bréon and Doutriaux-Boucher (2005) represented one of the first attempts to identify and understand the differences between the two techniques. The main finding from this study is that the bispectral-based MODIS retrieval of $r_e(2.13\mu m)$ (using the 2.13 µm SWIR band) is persistently larger than the polarimetric-based POLDER retrieval by about 2 µm over ocean, despite

5   a close correlation between the two. A variety of factors, from differences in sensitivity to cloud vertical profile to influence of cloud horizontal inhomogeneity, have been suggested to explain this difference. However, as pointed out by the authors, all these factors might contribute to the difference. It is difficult, if not impossible, to untangle them in observations and determine their relative importance. In addition, POLDER observations in this study were aggregated from the nominal 6 km spatial resolution to a much coarser 150 km resolution to achieve the angular resolution needed to resolve the cloud bow.

10   The vast difference in spatial resolution (i.e., 150 km for POLDER and 1 km for MODIS) makes the interpretation of the 2 µm r_e difference between the two retrievals even more difficult.

A more recent study by Alexandrov et al. (2015) is based on observations from the recent sub-orbital Polarimeter Definition Experiment (PODEX) in 2013. In that study, the polarimetric r_e retrievals for marine stratocumulus decks off the California coast from the airborne RSP instrument are compared to collocated bispectral retrievals from the Autonomous

15   Modular Sensor (AMS). Interestingly, the two retrievals are found to be in close agreement, with a correlation of 0.928 and negligible bias of less than a micron. Beyond the clear instrument differences of the Alexandrov et al. (2015) and Bréon and Doutriaux-Boucher (2005) studies, it is still unclear whether the bispectral and polarimetric retrievals should compare well to one another or not, raising numerous questions that motivate this study.

A great challenge facing these observational studies is the intertwining of various instrument and scene dependent

20   factors that lead to retrieval differences. For example, the polarimetric and bispectral methods have different sensitivity to the cloud vertical profile, and at the same time they are also both affected by cloud horizontal inhomogeneity (Miller et al., 2016; Zhang et al., 2012; 2016; Zinner et al., 2010). It is difficult, if not impossible, to disentangle these factors based on observations alone. This study approaches the intercomparison of bispectral and polarimetric retrievals through a different route: rather than use observational remote sensing data, synthetic retrievals are generated from large-eddy simulations

25   (LES) of clouds. Modeling radiative transfer in an LES scene to obtain total and polarized reflectances opens up the possibility of using the LES to perform synthetic bispectral and polarimetric retrievals. This retrieval simulator framework has proven to be a useful tool in other cloud remote sensing studies (Miller et al., 2016; Zhang et al., 2012). Using this idealized simulation at high spatial resolution, we can attempt to parse the effects of unresolved sub-pixel inhomogeneity, spatial resolution, and angular resolution on the intercomparison of polarimetric and bispectral retrievals. The use of a

30   satellite retrieval simulator opens up two unique opportunities for developing and studying cloud microphysical retrievals: First, it provides the means to compare retrievals directly to LES cloud microphysics. Second, it allows us to perform a retrieval technique intercomparison that is independent of instrument characteristics and other differences that complicate observational studies. This study focuses on three particular questions:

- How well do the bispectral and polarimetric retrievals perform relative to the LES fields used as input to the retrievals?
- How do the bispectral and polarimetric retrieval techniques compare to one another at high spatial resolution?
- How are the bispectral and polarimetric retrieval techniques sensitive to specific observational conditions (i.e., the influence of spatial and angular resolution)?

The rest of the paper is organized as follows: Section 2 provides a brief introduction to the theoretical basis of the two retrieval techniques; Section 3 describes the LES-based satellite retrieval simulations used in this study; the comparisons between the two techniques based on the LES cases are presented in Section 4; followed by summary and discussion in Section 5.

2 Background

2. Cloud microphysical and optical properties

In satellite remote sensing DSDs are often described using theoretical distributions that fit well with in situ observations, in addition to being mathematically convenient (Deirmendjian, 1964; Martin et al., 1994; Miles et al., 2000; Tampieri and Tomasi, 1976). A popular theoretical DSD is the gamma distribution proposed by Hansen and Travis (1974):

$$N\left(r\,;r_e,v_e\right) \equiv N_0 C r^{(1-3v_e)/v_e} \exp\left[-r/\left(r_e v_e\right)\right],$$ (1)

where the independent variable r is the cloud droplet radius, $N(r)$ is the droplet size distribution, N_0 is the droplet number concentration, and C is a normalization constant. The two distribution parameters are the effective radius (r_e) and the effective variance (v_e) of the DSD:

$$r_e \equiv \frac{\int_0^\infty Q_e(r) r^3 N(r) dr}{\int_0^\infty Q_e(r) r^2 N(r) dr} \approx \frac{\int_0^\infty r^3 N\left(r\,;r_e,v_e\right) dr}{\int_0^\infty r^2 N\left(r\,;r_e,v_e\right) dr} = \frac{\langle r^3 \rangle}{\langle r^2 \rangle},$$ (2)

$$v_e \equiv \frac{1}{r_e^2} \frac{\int_0^\infty Q_e(r)(r-r_e)^2 r^2 N(r) dr}{\int_0^\infty Q_e(r) r^2 N(r) dr} \approx \frac{1}{r_e^2} \frac{\int_0^\infty (r-r_e)^2 r^2 N\left(r\,;r_e,v_e\right) dr}{\int_0^\infty r^2 N\left(r\,;r_e,v_e\right) dr} = \frac{\langle r^4 \rangle \langle r^2 \rangle}{\langle r^3 \rangle^2} - 1.$$ (3)

where $\langle r^n \rangle = \int_0^\infty r^n N(r) dr$ is the nth moment of the DSD. For the spectral bands relevant to this study, the extinction efficiency (Q_e) is approximately constant (i.e., $Q_e(r) \sim \text{const.} = 2$). Thus, the relationships between r_e and v_e can be conveniently reduced to relations between arithmetic moments of the DSD. The DSD plays an important role in defining the bulk optical properties of a cloud. The optical property libraries used in this study are based on single scattering Mie calculations of monodisperse droplet optical properties that are averaged with respect to size, according to the gamma DSD (Wiscombe, 1979). In addition, these single-scattering optical properties are averaged with respect to wavelength over an instrument-

specific spectral response function (based on MODIS bands in this study) and solar source functions (Planck blackbody function (Planck, 1914)). The single-scattering bulk cloud optical properties are subsequently used to run radiative transfer calculations for the creation of the so-called bispectral reflectance look-up-table (LUT). This LUT is made up of pre-calculated reflectances of plane-parallel and homogeneous (PPH) clouds over a high-resolution grid of combinations of τ, r_e,

5 and v_e. Here, τ is defined in terms of the DSD:

$$\tau_{tot,\lambda} \equiv \int_{TOA}^{0}\left[\int_{0}^{\infty} Q_{e,\lambda}(r)\pi r^2 N_0 n(r)dr \right]dz$$

(4)

2.2 Bispectral and Polarimetric Retrieval Methods

The bispectral method retrieves τ and r_e simultaneously from a pair of cloud reflectances observed in VNIR and

10 SWIR bands, respectively. The VNIR band, dominated by multiple scattering, provides sensitivity to τ; the selected SWIR band, where liquid water droplets are moderately absorptive, provides sensitivity to r_e. This method is usually implemented using a LUT like the one shown in Figure 1 (a), which has a fixed v_e. Cloud reflectance in the VNIR band (centered around 0.865 μm) increases with τ (gray) for a fixed r_e, while the reflectance in the SWIR band (centered around 3.75 μm) decreases with r_e (colored) when τ is fixed. The retrieved properties are obtained by performing a two-dimensional inverse

15 interpolation between observed reflectance and the τ-r_e grid. A notable characteristic of the bispectral LUT is that when the optical thickness is low (τ<3), the isolines of the LUT are more densely packed and less orthogonal, which results in reduced sensitivity and increased retrieval uncertainty (Werner et al., 2013). The bispectral technique is not particularly sensitive to v_e, so typically a fixed a priori value is assumed (e.g., v_e=0.1 in the operational MODIS retrieval). While different combinations of VNIR and SWIR bands are used to perform the bispectral retrieval, in this study we focus on VNIR

20 reflectances centered on 0.865 μm and SWIR reflectances centered on both 2.13 and 3.75 μm. There are consequences for the r_e retrieval depending on the particular SWIR band selected. For example, a strongly absorbing band limits penetration into the cloud and as a result the retrieved r_e is vertically weighted toward the microphysics prevalent in the uppermost part of the cloud (Platnick, 2000).

For the polarimetric retrieval, the angular pattern of the linearly polarized reflectance[1] is the source of sensitivity to

25 cloud microphysical properties. Polarized reflectances are dominated by single scattering because multiple scattering induces depolarization. As a result, the single-scattering polarized phase functions ($-P_{12}$) shown in Figure 1 (b) and (c) are good approximations to the observed angular pattern of polarized cloud reflectances (Bréon and Goloub, 1998). These phase functions demonstrate the sensitivity of the polarimetric retrieval to both r_e and v_e. As r_e increases in Figure 1(b) the supernumerary bow peaks (around a scattering angle of 142°) become narrower and shift toward smaller scattering angles. In

---

[1] Note that throughout this paper, we will refer to "linearly polarized reflectances" simply as "polarized reflectances" in recognition of the negligible contribution of circularly polarized light in the atmosphere (Hansen, 2010).

contrast, as v_e increases in Figure 1(c) the supernumerary bow peaks erode in magnitude, eventually smoothing out for broad DSDs ($v_e > 0.15$). A consequence of this erosion of the supernumerary peaks is that the polarimetric retrieval has less sensitivity to both r_e and v_e for very broad DSDs. The polarimetric retrieval does not significantly rely on multispectral information, although observations in several bands may help provide stronger observational constraints due to the shift in

5   the supernumerary bows with changing wavelength (refer to figure 3 of Bréon and Goloub (1998). The dominance of the single scattering contributions to the polarized reflectance leads to cloud retrievals that represent microphysical properties within the top ~3 optical depths in the cloud. The polarimetric retrieval is often based on a parametric curve fitting retrieval algorithm like the one presented in Alexandrov et al. (2012b), although there are other techniques (e.g., the Rainbow Fourier Transform technique of Alexandrov et al. (2012a), which can retrieve multi-modal DSD's.) The parametric technique relies

10   on a library of $-P_{12}$ curves with varying r_e and v_e that are parametrically scaled and adjusted to fit the observed reflectance via a nonlinear least squares optimization procedure. This process yields the phase function that best matches the angular pattern of the observation, thus determining the r_e(pol) and v_e(pol) retrieval. The polarimetric method described above does not result in a retrieval of τ; however, it can still be obtained by implementing a simplified variant of the bispectral τ retrieval. With simultaneous measurements of the total reflectance in a VNIR band and the r_e(pol) retrieval, a VNIR-only LUT curve

15   can be used to perform a 1-D interpolation of the corresponding bispectral LUT curve for $R_{\text{VNIR}}(r_e(\text{pol}), \tau)$.

Both bispectral and polarimetric techniques are susceptible to a variety of retrieval uncertainties. The main objective of this study is to understand how the retrieval uncertainties influence each technique and whether they can lead to deviation between the two techniques in terms of retrieval results. In this study, we focus on three major sources of retrieval uncertainty for both techniques:

20   1) Cloud vertical profile: In the operational retrievals, both bispectral and polarimetric techniques assume vertically homogenous clouds. However, clouds in reality often have significant vertical variability resulting from various processes (e.g., condensational growth, coalescence, sedimentation, entrainment). Deviations from the assumed profile gives rise to many questions. For example, how do we interpret the r_e and v_e retrievals based on the homogenous cloud assumption? To what extent does cloud vertical profile influence the bispectral and polarimetric techniques? Note that Platnick (2000)

25   developed a method utilizing the so-called "vertical weighting function" to interpret the r_e retrieval from the bispectral method for clouds with vertically varying r_e profile. Recently, Alexandrov et al. (2012b) modified this method slightly and applied it to interpret the r_e and v_e retrievals from the polarimetric technique. Miller et al. (2016) demonstrated the usefulness of this vertical weighting approach for understanding both bispectral and polarimetric r_e retrievals. In Section 4.1, we will apply the vertical weighting function method to both techniques on the basis of the LES cloud fields, to help understand if

30   cloud vertical structure could lead to significant differences between the two techniques.

2) Reduced sensitivity: It can be clearly seen from Figure 1 (a) that when clouds are optically thin ($\tau < 3$), the LUT for the bispectral retrieval becomes less orthogonal and the isolines of r_e become more densely packed. This reduction in sensitivity can lead to significant retrieval uncertainties in bispectral techniques for optically thin clouds ($\tau < 3$). Similarly, the sensitivity of the polarimetric technique to r_e and v_e is reduced when DSD becomes very broad (i.e., $v_e > 0.15$), in which case

the supernumerary bow features are barely distinguishable (Figure 1 (c)). In Section 4.2 we will investigate the impacts of the reduction of sensitivity on retrieval consistency between the two techniques.

3) Sub-pixel inhomogeneity: The impact of spatial resolution and unresolved sub-pixel cloud inhomogeneity on bispectral retrievals has been well studied (Zhang and Platnick, 2011; Zhang et al., 2012; 2016). An important conclusion

5   from these studies is that the so-called plane-parallel homogenous bias (PPHB) can cause the bispectral technique to significantly overestimate r_e. In contrast, the sensitivity of the polarimetric retrieval to unresolved sub-pixel inhomogeneity and resolution has not been thoroughly studied. In Section 4.3, we will compare the impacts of sub-pixel inhomogeneity on bispectral and polarimetric techniques, and investigate whether it can cause deviation between the two techniques.

4) Angular resolution and sampling for polarimetric technique: In addition to spatial resolution, angular resolution

10   and sampling is also important for the polarimetric technique. A coarse angular resolution may not be able to resolve the feature of the supernumerary bows. Similarly, if the scattering angles corresponding to the supernumerary bows are not or only partly sampled, then the polarimetric technique may not have enough information content for retrieval. This issue will be discussed in Section 4.4.

15   **3 Model and Methodology**

The satellite retrieval simulator implemented in this study is built around an LES model (DHARMA) with bin microphysics (Ackerman et al., 2004; Miller et al., 2016; Zhang et al., 2012). The LES provides freely evolving 3-D cloud microphysical properties, which are used as reference when comparing to numerically simulated retrievals. The LES in this study adopts 25 droplet size bins to represent droplet size distributions (*Ackerman et al.*, 1995). The optical properties of

20   each size bin are computed by bulk averaging Mie scattering properties over a highly resolved flat sub-bin droplet size distribution. The optical properties of each bin are provided as input to radiative transfer simulations based on the size distributions of the LES cloud fields. Vector radiative transfer calculations are performed using a polarized doubling-adding technique (PDA) to produce 1-D total and polarized reflectances at the horizontal resolution of the LES grid (described below) (De Haan et al., 1987). The sole consideration of 1-D retrievals avoids 3-D radiative effects and focuses this study on

25   retrieval technique differences rather than on radiative processes. A future study will focus on the comparison of 3-D retrievals to these 1-D bispectral and polarimetric retrievals. The radiative transfer modeling in this work is performed for numerous solar zenith angles (SZA=[20, 40, 60]°), viewing zenith angles (VZA=[−70 : +70]°), and a constant relative azimuthal angle (ΔΦ = 30°). The VZA resolution results in a scattering angle (Θ) resolution on the order of 0.5°. Reflectances in spectral bands (based on MODIS spectral response functions) are centered on 0.865, 2.13, and 3.75 μm

30   wavelengths. Total reflectances in all bands are used to produce bispectral retrievals, whereas linearly polarized reflectances in the 0.865 μm band are used to produce polarimetric retrievals. Subsequently, bispectral and polarimetric retrievals are performed on the simulated reflectances to obtain r_e, v_e, and τ retrievals. Bispectral and polarimetric retrievals are performed over a subset of observation geometries, with bispectral retrievals performed for VZA=[50, 40, 30, 20, 10, 0, −10]° and all

SZA. Meanwhile, the polarimetric retrievals are performed for a SZA=20° and a range of VZA=[0:27]° that result in reflectances spanning scattering angles required to observe the primary and supernumerary bow features (i.e., Θ=[135:160]°). Reflectances are also aggregated from the 50 m native LES resolution up to coarser 100, 200, 400, and 800 m horizontal resolutions to reflect the influence of different remote sensing footprints. The retrievals in this study are also

5   performed at all of the footprint resolutions. The bispectral LUT implemented in this study spans microphysical properties r_e=[2:30] μm in steps of 0.5 μm and v_e=[0.01:0.11] in steps of 0.01. The τ retrieval in this study is anchored to the 0.865 band optical properties and spans τ=[0.1:100] with 101 logarithmically spaced grid points. Including v_e variability in the bispectral LUT allows for the comparison of standard MODIS-like retrievals (the v_e=0.1 LUT) to retrievals with other v_e assumptions. The bispectral retrieval is then accomplished by performing a 2-D linear interpolation of the observed

10   reflectances and inverting between the reflectance and retrieval space. For the polarimetric retrieval, the polarimetric phase function library spans r_e=[2:40] μm in steps of 0.25 μm and v_e=[0.01:0.3] in steps of 0.01. The polarimetric retrieval implemented in this study is based on the approach of Alexandrov et al. (2012a), fitting the polarized phase functions in their eq. (3) to the modeled polarized reflectances of the LES scene. The optimal parametric fit in the $-P_{12}$ library is determined by using the Levenberg-Marquardt nonlinear least squares algorithm. This optimally fitting phase function corresponds to

15   the resulting r_e(pol) and v_e(pol) retrieval. As previously stated in section 2.2 the polarimetric retrieval of τ is accomplished by using a constrained 1-D version of the bispectral LUT.

       The LES cloud fields are used not only to drive the radiative transfer simulations, but also to help interpret and understand the retrieval results. As mentioned in Section 2.2, it is not trivial to interpret the r_e and v_e retrievals based on the homogenous cloud assumption when the cloud has significant vertical structure. To address this issue, for each LES column

20   with detailed vertical profiles of DSD, we derive two reference variables r_e(2WT) and v_e(2WT) from the vertical integration of the DSD profile. The integration is weighted by a two-way transmittance (2WT) function to account for the penetration depth of the single-scattered radiation (at 0.865 μm). For a complete description on how vertical weighting is accounted for in the calculation of r_e(2WT) and v_e(2WT), see section 2 of (Miller et al., 2016). The r_e(2WT) and v_e(2WT) take into account the first-order sensitivity of the retrieval techniques to the vertical profile of clouds. Thus, they are directly comparable to the

25   numerically retrieved r_e and v_e from the simulated reflectance (Alexandrov et al., 2015; Miller et al., 2016; Platnick, 2000; Zhang et al., 2010). We note that the 2WT vertical weighting function provides a reasonable approximation when the signal is contributed mainly by single scattering (i.e., 3.7 μm or polarimetric reflectances) but becomes less accurate for spectral bands with more multiple scattering (Platnick, 2000). In addition to r_e(2WT) and v_e(2WT), we also derive τ_{LES} for each LES column simply by integrating the extinction coefficient from cloud bottom to cloud top. The r_e(2WT), v_e(2WT) and

30   τ_{LES} are used as references in the retrieval and LES property comparison in Section to understand the differences between the retrievals and the original LES fields. After obtaining the r_e(2WT), v_e(2WT) and τ_{LES} at the 50 m native LES resolution, they are aggregated to 100, 200, 400, and 800 m to help interpret the retrievals at these coarser resolutions. It is important to

note that there is a subtle difference between directly aggregating r_e(2WT) or v_e(2WT), and aggregating the DSD (i.e., $N(r)$) first and then deriving the corresponding r_e(2WT) and v_e(2WT). The differences between the two methods are discussed in the Appendix. The main conclusion is that, although the two aggregation methods could be different in some hypothetical cases that have unrealistically large small-scale variation of DSD (Shang et al. 2015), they are essentially equivalent for

5   practical purposes. In this study, we simply aggregate r_e(2WT) and v_e(2WT) from the native LES resolution of 50 m to obtain the values at desired resolution (e.g., 800 m).

Three LES cases are the focus of this study. The first (referred to as "ATEX clean" hereafter) and second ("ATEX polluted") cases are based on an idealized case study from the Atlantic Trade Wind Experiment (ATEX), with different aerosol loadings (Stevens et al., 2001). The ATEX cases are representative of a trade wind cumulus regime in which

10   scattered cumuli rise into a thin, broken stratocumulus layer. The third case (referred to as "DYCOMS-II" hereafter), originally presented in Stevens et al. (2005), is an idealized setup based on clouds observed during the second research flight (RF02) of the Second Dynamics and Chemistry of Marine Stratocumulus project (DYCOMS-II) (Stevens et al., 2003). This case is representative of nocturnal marine stratocumulus under a dry inversion. The DYCOMS-II case has a domain size of 6.4×6.4×1.5 km (128x128x96 grid points), while each of the ATEX simulations has a domain size of 7.2×7.2×3 km

15   (144×144×200 grid points). The horizontal grid spacing of these LES cases is fixed at 50 m, while the vertical grid is stretched, with a minimum spacing of 5 m near the surface and the capping temperature inversion to better resolve small-scale turbulence there. Further details of the model setup for the DYCOMS-II case are provided in Ackerman et al. (2009). The ATEX cases are updated model runs with increased spatial resolution that are similar to the cases discussed in Fridlind and Ackerman (2011). For each LES scene a snapshot of cloud microphysical and optical properties is saved every half hour

20   after the first hour of each simulation, resulting in numerous cloud fields. A single time step of each of the cases was selected to be the focus of this retrieval study, each occurring ~3 hours into the simulation.

The variability of cloud optical and microphysical properties in each of the LES cases is highlighted in Figure 2 and Table 1. Spatial inhomogeneity of both optical and microphysical properties of these scenes is evident, with the ATEX polluted and DYCOMS-II cases exhibiting lower spatial inhomogeneity and the ATEX clean case being more broken and

25   inhomogeneous. One method for quantifying the optical inhomogeneity of a cloud scene is to use the sub-pixel inhomogeneity index,

$$H_\sigma(\text{resolution}) = \frac{\text{std}\left[R_i(0.865\ \mu m, 50\ m)\right]}{\text{mean}\left[R_i(0.865\ \mu m, 50\ m)\right]}, \tag{4}$$

where the numerator and denominator are the standard deviation and mean of the native LES resolution (50 m) reflectances within a coarser resolution pixel. Thus, the value of H_σ is computed at a coarser spatial resolution (800 m in Table 1) and

30   increases with increasing pixel inhomogeneity. In addition to optical inhomogeneity, each of the LES scenes also has characteristically different microphysical properties. The average value of r_e(2WT) of each scene varies, in part because of the initial background CCN in each particular case but also cloud top height variability. In these LES cases v_e is spatially

anti-correlated with τ and organized in a cellular structure — regions with higher τ tend to have smaller v_e(2WT) and regions with lower τ tend to have large v_e(2WT).

4 Results and Analysis

5 ### 4.1 Retrieval and LES Property Comparison

Before comparing the retrieval results from the two techniques, in this section we first carry out a comparison of LES and retrieval properties to assess and understand the differences between the retrieval results and the original LES cloud fields at the native 50 m spatial resolution. This is a necessary sanity check that will help understand the accuracy and uncertainty of our retrieval routines. More importantly, this study will help to interpret the retrievals based on homogeneous

10 cloud assumption when the LES cloud fields have significantly inhomogeneous vertical profiles.

The bispectral retrieval comparison to LES properties in Figure 3 depict joint histograms of r_e and τ retrievals using both the 2.13 and 3.75 μm SWIR bands against the reference values derived from the LES fields, r_e(2WT), v_e(2WT), and τ_{LES}. The two bispectral r_e retrievals, r_e(2.13 μm) and r_e(3.75 μm), are in agreement with the LES ground-truth (Figure 3(a) and (b)) with strong correlations, both exceeding 0.95. The biases between these two retrievals and the LES properties differ

15 slightly. As expected from the vertical weighting differences discussed in section 2.2, the 2.13 μm retrieval is typically smaller than the 3.75 μm retrieval. Both r_e retrievals have relatively small mean biases of less than a micron compared to LES. The mean absolute biases are also less than 1 μm. Note that the mean regression biases reported throughout this study are stated relative to the plotted axes as, $\mu_{\text{bias}}=\langle y-x\rangle$ and $\mu_{|\text{bias}|}=\langle|y-x|\rangle$ (i.e., x and y denoting x and y axes). Additionally, it is important to note a limitation of this population: none of the LES scenes in this study have a mean cloud top r_e near 10

20 μm. The two bispectral τ retrievals, τ(2.13 μm) and τ(3.75 μm) in Figure 3(c) and (d), are compared here in terms of percent differences. Each of these τ retrievals also reveal good correlations (R>0.99), despite a slight high bias on the order of 2-5%. As explained earlier in Section 2.2, the bispectral method suffers a reduction of sensitivity when clouds are optically thin. By sampling only LES columns that are optically thick (τ>3) a substantial improvement in the regression correlations of the two r_e retrievals (Figure 3(e) and (f)) is achieved. However, some outlier points still remain. In particular, both r_e(2.13 μm) and

25 r_e(3.75 μm) have some cases where the retrieved values (10 ~ 30 μm) are substantially larger than the corresponding r_e(2WT) values (mostly around 5 μm). The cause of these outliers and some other differences between the retrievals and LES fields will be discussed in detail in section 4.2.

The joint histograms in Figure 4 depict comparisons of the polarimetric retrievals, r_e(pol) v_e(pol), and τ(pol), against corresponding LES properties. The r_e(pol) retrieval compares very well to r_e(2WT) (Figure 4(a)), with a regression

30 correlation exceeding 0.98 and a mean bias of less than 0.1 μm. The quality of this retrieval comparison to LES properties also supports the definition of r_e(2WT), as the polarimetric retrieval is indeed well represented by the single-scattering "2WT" vertical weighting. In contrast, the polarimetric retrieval of v_e(pol) reveals a regression against v_e(2WT) (Figure 4(c))

that does not perform quite as well. In this case the regression correlation is much weaker (0.62) with a mean bias of −0.013. While the mean bias is on the order of the v_e LUT grid spacing, it is clear that the regression correlation is poor because of a systematic low bias for v_e(2WT) larger than about 0.15 (footnote 2). Comparing only the population with v_e(2WT)≤0.15 (not shown here) results in an improved correlation of 0.86 with negligible mean bias. The final retrieval product, τ(pol) (Figure

5   4(e)), indicates that more accurate a priori r_e and v_e estimates have little impact on the retrieval of τ. As explained earlier in Section 2.2, the polarimetric method suffers a reduction of sensitivity when the DSD is broad. This explains, for the r_e(pol) retrieval, why limiting the regression population to LES columns with v_e(2WT)≤0.15 in Figure 4(b) increases the correlation and decreases the absolute bias. This appears to be an indication of sensitivity to degradation of the supernumerary bow features for large v_e, features that are necessary for reliable r_e(pol) and v_e(pol) retrievals. For v_e(pol) we find that by

10   sampling LES columns that are optically thick (τ>3), there is moderate improvement in the correlation and reduced biases (Figure 4(d)). This improvement stems from the correlation between the population of optically thin clouds and high v_e(2WT) (Figure 4(f)) that are found near cloud edges in the LES scenes. It should be noted that an increased τ does not implicitly lead to better polarimetric retrievals, but here it is observed to be a consequence of aforementioned correlated relationship between DSD and optical properties.

---

2 The increased concentration of v_e(pol) retrievals at v_e=0.3. is a result of the boundaries of the retrieval space, v_e=[0.01, 0.3]. This limitation is a consequence of the definition of the modified gamma distribution in Hansen and Travis (1974); for v_e=0.3 the size distribution becomes monotonic.

4.2 Retrieval Comparison at High Resolution

At the native spatial resolution of the LES (50 m) direct intercomparisons of polarimetric and bispectral retrieval techniques offer the possibility of diagnosing different sources of bias. The joint histograms of r_e retrievals in Figure 5

5 compare the two bispectral retrievals, r_e(2.13 µm) and r_e(3.75 µm), to the polarimetric retrieval, r_e(pol), for all LES cases and observation geometries[3]. The regressions for the comparison of both r_e(2.13 µm) (Figure 5(a)) and r_e(3.75 µm) (panel b) indicate high correlation (R≈0.954) and have relatively small mean biases of less than a micron. A couple of notable features are evident in these regressions. **(1)** The sign of the mean bias appears to be sensitive to the SWIR band selection due to vertical weighting differences, resulting in r_e(2.13µm)<r_e(pol)<r_e(3.75µm). **(2)** There are numerous statistical outliers with

10 small r_e(pol)~5-9 µm but broadly distributed r_e(2.13 µm) or r_e(3.75 µm). One way to understand these features is to constrain the data set to LES columns where both retrieval techniques yield reliable results. As discussed previously, both the bispectral and polarimetric retrievals are sensitive to biases for thin clouds (τ<3) and the polarimetric retrieval is sensitive to biases for broad droplet size distributions (v_e>0.15). Based on these criteria (τ>3 and v_e≤0.15), the constrained joint histograms (Figure 5(c) and (d)) feature much tighter regression relationships (R≈0.99) and reduced mean absolute biases are

15 observed. These filters indicate that the poorly correlated population corresponds to situations in which both retrievals are expected to suffer from significant biases. The retrieval regression can be further improved if the bispectral retrieval is artificially provided with more complete information about the shape of the droplet size distribution. Providing the v_e(pol) retrieval as an a priori assumption for the bispectral LUT can demonstrate the sensitivity of the bispectral r_e retrievals to the v_e=0.1 assumption. To create these new retrieval results we coupled the selection of the bispectral retrieval LUT to the pixel-

20 by-pixel value, thus making sure that the respective LUT had a matching v_e to the v_e(pol) retrieval. The new r_e(2.13 µm) retrievals (Figure 5(e)) are largely unchanged from the v_e=0.1 results, although a slight increase in the two biases indicates that v_e=0.1 was both an appropriate and sufficient assumption for the r_e(2.13 µm) retrieval. In contrast, the r_e(3.75 µm) retrieval (Figure 5(f)) is shown to benefit from this additional a priori information, improving the correlation and reducing the small systematic low bias (~0.25 µm). The differences between the two SWIR band retrievals can be explained in two

25 ways. Firstly, the vertically weighted DSD of the 2.13 µm SWIR band might result in a broader DSD (i.e., a larger v_e) compared to the 3.75 µm SWIR band, due simply to deeper penetration into cloud. This could provide one explanation for why the r_e(2.13 µm) retrieval might improve with the v_e=0.1 assumption. Alternatively, the R(2.13 µm) reflectance might simply be less sensitive to the broader DSD shape than the R(3.75 µm) reflectance. Overall, these results demonstrate a feature well known to the remote sensing community; the bispectral retrieval of r_e is not particularly sensitive to v_e

30 (Nakajima and King, 1990a). Indeed, comparison of the coupled bispectral retrieval of r_e to the polarimetric retrieval of r_e

---

[3] Note that ~1% of pixels in the LES retrieval data correspond to a "failed" bispectral retrieval due to falling outside of the LUT space. These pixels are omitted from the intercomparison. Different reasons for bispectral retrieval failure are discussed in (Cho et al., 2015).

confirms that the advantage of retrieving v_e changes the bispectral retrieval of r_e by less than a micron, so it is appropriate to neglect this level of detail of the DSD for bispectral retrieval purposes. The slight improvement demonstrates that when the two retrievals are compared on equal information footing they are nearly equivalent.

5   The origin of the broadly distributed high-biased bispectral retrievals in the small droplet size regime (r_e(pol)~5 μm) stems from the ATEX polluted case, where such small droplets make up about 5% of the LES scene[4]. A close examination of this case reveals that there are no bispectral retrievals below 5 μm, despite approximately 5% of the cloudy pixels (as defined by $\tau_{LES} > 0.1$) in the scene being characterized by r_e(2WT)<5μm. This feature is a consequence of the bispectral LUT state space[5], which covers a r_e range of 5-30 μm. In contrast, the polarimetric retrieval space covers 1-30 μm. The differences between these two LUT spaces is not so much a matter of decision-making, but is more reflective of

10   complexities of the bispectral retrieval for small r_e. To demonstrate this point panels (a) and (b) of Figure 6 depict the cloud reflectances from the ATEX polluted case (colors) within the respective bispectral LUT. It is obvious that the black isolines for τ and r_e increasingly overlap with the standard LUT space as τ decreases. In this region of the state space, there are multiple solutions for a single reflectance pair; one solution is representative of a small r_e (<5 μm, extended LUT), while the other indicates a much larger r_e (≥5 μm, standard LUT). There is also a modest impact on τ, but due to the curvature of the

15   LUT this impact is less severe. The overlapping region between the standard and extended LUT is referred to as the "multiple solution space" and the amount of LUT overlap is determined by both the observation geometry and the selected spectral bands. Depending on the optical thickness, the larger r_e retrieval may be significantly larger, because the extended LUT isolines cross numerous larger r_e isolines in the standard LUT. The associated r_e(SWIR)−r_e(2WT) retrieval bias, shown in Figure 6(c) and (d), highlights the conclusion that for optically thick clouds the bispectral r_e retrievals exhibits only

20   moderate retrieval biases on the order of ±1 μm. However, for very thin clouds (near cloud edge) the retrieval bias can increase significantly. For some of these thinner clouds the retrievals also fall within the multiple solution space, so it is possible to attribute the very large biases to the presence of ambiguous retrieval results. Furthermore, the multiple solution space also provides an additional explanation for why the removal of optically thin (τ<3) observations significantly improved the bispectral retrieval comparisons.

25   In contrast to the intercomparison of r_e retrievals, the τ retrieval intercomparison in Figure 7 reveals very few differences between the bispectral and polarimetric techniques. This is not surprising, because the τ(pol) retrieval is simply an implementation of the bispectral technique with additional constraints on r_e and v_e (as discussed in section 2.2).

---

[4] Additionally, ~2.5% of the cloudy pixels in this scene exhibit values below 4 μm.
[5] Note that the MODIS LUT extends its range down to 4 μm, and in situations with multiple solutions the larger retrieval value is selected.

4.3 Sensitivity to Unresolved Spatial Inhomogeneity

Unresolved spatial inhomogeneity affects the bispectral and polarimetric cloud retrievals in very different ways. These retrievals exhibit different sensitivities to sub-pixel inhomogeneity even for 100% cloudy pixels. As coarsened spatial resolution and the sub-pixel inhomogeneity index (H_σ) are inherently correlated with one another, so our comparisons here

5   address these two properties simultaneously. To that end, panels (a) and (b) of Figure 8 compare r_e(pol) to the r_e(2.13 µm) and r_e(3.75 µm) respectively at increasingly coarsened spatial resolutions (as indicated by the size of the circles). In addition to the spatial resolution, these plots also indicate the magnitude the of sub-pixel inhomogeneity index (H_σ) (as indicated by the color of the circles). It is evident that as the spatial retrieval footprint reaches 800 m the sub-pixel inhomogeneity tends to increase and the r_e(2.13 µm) retrieval suffers from an increasingly high bias relative to the polarimetric retrieval. The

10   presence of this behavior is less pronounced for in the r_e(3.7 µm) comparison is lower, although the trend is still clearly present.

To probe how unresolved inhomogeneity influences these two retrieval techniques, we will examine a particularly inhomogeneous pixel from the ATEX clean case at a very coarse resolution (800m). Focusing first on the bispectral retrieval using the 2.13 µm SWIR band, the LUT scatterplot in Figure 9(a) reveals that there is significant variability in the sub-pixel

15   (i.e., 50 m) VNIR reflectances, indicated by a large value of the sub-pixel inhomogeneity index (H_σ=0.5637). In contrast to the variability of VNIR reflectances, the microphysical properties of this 800 m pixel are largely homogeneous, indicated by the narrow distribution of sub-pixel r_e(2WT)$_{50\,m}$ (color of the points). The sub-pixel mean of $<r_e$(2WT)$>_{50\,m}$ =19.23 µm agrees well with the mean of both sub-pixel retrievals, $<r_e$(2.13 µm)$>_{50\,m}$=18.73 µm and $<r_e$(pol)$>_{50\,m}$=18.92 µm. This combination of optical inhomogeneity and microphysical homogeneity leads to an average reflectance (indicated by the

20   black star) for the 800 m pixel that falls significantly below the r_e=20 µm isoline (i.e., the closest isoline to the mean sub-pixel retrievals). Thus, the coarse resolution 800 m reflectance results in an 800 m bispectral retrieval with r_e(2.13 µm)$_{800\,m}$=23.62 µm, which is biased high by ~4 µm. This effect is attributable to the well-documented PPH bias induced by the curvature of the bispectral LUT with respect to the optical thickness (Zhang and Platnick, 2011; Zhang et al., 2012; 2016). The PPH bias has a stronger influence on the 2.13 µm retrieval compared to the 3.75 µm retrieval because the

25   curvature of the LUT is more pronounced.

The polarimetric retrieval has a fundamentally different relationship to the unresolved sub-pixel inhomogeneity, as shown in the sub-pixel polarized reflectance histogram in Figure 9(b). The reflectances in this figure have been binned by scattering angle to demonstrate the 50 m sub-pixel distribution of polarized reflectances within the selected 800 m pixel footprint. Within the plot there are also two curves, shifted in amplitude away from the histogram for clarity, that display the

30   mean 800 m multi-angular polarized reflectance and the corresponding 800 m retrieved polarized phase function. It is evident from this histogram and these curves that the mean angular position of the supernumerary bow does not shift, indicating that there is no significant difference between r_e(pol)$_{800\,m}$, $<r_e$(pol)$_{50\,m}>$, and $<r_e$(2WT)$_{50\,m}>$. In contrast, there is clear variability in the amplitude of sub-pixel polarized reflectances. This variability owes itself to both optical (τ), and

microphysical inhomogeneity (i.e., v_e(2WT)>0.15) within the coarse resolution pixel. For thin clouds (τ<3) the supernumerary bow amplitude is dependent on both τ and v_e. With a fixed v_e and varying τ the polarized reflectance converges towards an asymptotic maximum for optically thick clouds (τ≥3), a consequence of increasing depolarization due to multiple scattering. Similarly, for a fixed τ, reflectances corresponding to v_e(2WT)>0.15 also produce decreased

5 polarization in the primary and supernumerary bow features, as discussed in section 2. Despite the fact that both types of inhomogeneity induce an asymmetric polarized reflectance distribution, we find that these features do not systematically bias the v_e(pol) retrieval in this case. In fact, rather surprisingly, we find that the most important bias for the coarse spatial resolution v_e(pol) retrieval is the lack of sensitivity on v_e(2WT)>0.15, a feature that was also present for the high spatial resolution retrievals. This finding is also supported for polarimetric retrievals performed on subsamples of the polarized

10 reflectance of this 800 m pixel that omitted either the v_e(2WT)>0.15 or τ<3 from the population; removing either of them had little to no impact on either the coarse resolution r_e(pol) or v_e (pol) retrieval. Possible explanations for this behavior will be discussed in section 5.

4.4 Sensitivity to Angular Resolution and Sampling

15 The polarimetric retrieval requires high-resolution multi-angular data to resolve the supernumerary bow features. To test how angular resolution influences polarimetric retrievals we examined coarse spatial resolution (800 m) r_e(pol) retrievals at different angular resolutions. Each angular resolution (i.e., changing angular step size) was also convoluted with shifting angular sampling (i.e., changing the initial angle). This convolution is necessary in order to account for all possible sets of scattering angle observations associated with each resolution. These coarse resolution retrievals were then compared

20 to the original high angular resolution retrieval. The results of this experiment (**Figure 10**(a)) reveal that coarsening angular resolution does not systematically bias r_e(pol) retrievals, although angular resolutions exceeding 3° do result in a marked increase in retrieval variability (i.e., a constant mean bias, but increased absolute bias). In contrast, **Figure 10**(b) demonstrates that angular resolutions exceeding 3° lead to both high-biased v_e(pol) and increased retrieval variability. An explanation for the origin of the observed degradation in retrieval accuracy above 3° angular resolution is demonstrated in Figure 11(a). Two

25 different polarized phase functions with r_e=15 μm and v_e=[0.03, 0.2] (solid and dashed-dotted, respectively) are sampled at an angular resolution of 3.5° (indicated by the gray vertical lines). This resolution is coarser than the spacing between the supernumerary bow features. As a consequence, this particular angular sampling intersects these curves at nearly the same amplitudes. This degeneracy yields a relatively low cost function during the best-fit optimization step of the polarimetric curve fitting retrieval algorithm, making it possible to obtain an inaccurate solution if this results in a cost-function

30 minimum. The lack of observed differences between these two curves results in a lack of v_e information. However, under different angular sampling conditions, e.g., shifting the initial angle by a few degrees to the right, the supernumerary bow peaks of the low v_e curve would be sampled and the similarity between the observations of these two curves would vanish. This example highlights an important feature of multi-angular polarimetry: observations at poor angular resolutions can

suffer from increased biases depending on whether or not important angles are sampled. Generalizing this result requires determining the angular spacing of the supernumerary bow features for other r_e. Pursuing this, we find that decreasing cloud droplet size widens and dilates supernumerary bow features, making it easier to resolve supernumerary bow features at coarse angular resolution. The peak-to-peak distance of the supernumerary bow oscillations can be treated as the Nyquist

5   frequency, or in this case Nyquist resolution. In signal analysis, a sampling resolution finer than the Nyquist frequency is required to appropriately resolve features of an oscillatory signal. The Nyquist angular resolution required for resolving the supernumerary bow oscillations changes with both r_e and λ according to the behavior illustrated in Figure 11(b). This analysis indicates that multi-angular observations in a shorter wavelength spectral band would require finer angular resolutions. The Nyquist angular resolution for λ=0.865 and r_e=15 μm is 3°, providing an explanation for the increased

10   uncertainty in r_e(pol) and v_e(pol) LES retrievals at angular resolutions coarser than the Nyquist limit.

5 Summary and Discussion

The analysis in this study, which features comparisons of vastly different passive cloud property retrieval techniques, is facilitated by comparisons to LES cloud fields used as input to the retrievals. At the native LES resolution (50 m) there are

15   promising results for both the bispectral and polarimetric retrievals. For the bispectral retrieval, the LES comparison shows significant biases for retrievals of very thin clouds, as well as only small differences between the vertically weighted cloud properties in each of the two SWIR bands (2.13 and 3.75 μm). Meanwhile, for the polarimetric retrieval, the comparison demonstrates that the r_e(pol) retrieval agrees well with the vertically weighted in situ properties of each LES scene. However, the v_e(pol) retrieval exhibits persistent low biases due to a lack of retrieval sensitivity to very broad droplet size

20   distributions (i.e., v_e(2WT)>0.15). The optical thickness retrievals from both methods are effectively the same, with the caveat that the polarimetric technique performs the r_e(pol) retrieval as an a priori constraint on the τ retrieval space. Regarding τ, both bispectral and polarimetric retrievals were found to have a small systematic high bias on the order of 2-5%.

The retrieval intercomparison of polarimetric and bispectral retrievals in this study demonstrates that both techniques

25   yield very similar results, especially when the most reliable populations of cloud properties are selected for each method (τ>3 and v_e around 0.1). While the physical principles and measurement requirements are vastly different, both retrieval techniques seem to be able to capture similar information about r_e. These results agree with high-resolution airborne observations obtained during the PODEX and ORACLES field campaigns, where RSP and AMS microphysical retrievals are compared (Alexandrov et al., 2015; Knobelspiesse et al., 2017). These high spatial resolution field campaign

30   observations indicate that the two retrieval techniques agree well to within the tolerances also found in the present study. The bispectral r_e retrievals are found to be moderately sensitive to v_e in the 3.75 μm band, and less so in the less absorptive 2.13 μm band. Coupling the retrieved v_e(pol) to the bispectral r_e(3.75 μm) retrieval led to slight improvements in the r_e(pol) and r_e(2WT) comparison. It should be noted that for MODIS cloud products the bias due to the v_e=0.1 assumption does not

substantially impact the r_e retrieval compared to other sources of bias (i.e., cloud inhomogeneity or 3-D radiative effects). In addition, the MODIS Collection 6 cloud product includes uncertainty estimates associated with the v_e assumption. The intercomparison of the bispectral and polarimetric τ retrievals indicates that the two produce very similar results. This was to be expected, as the polarimetric technique also uses a bispectral LUT approach to derive τ. When the results from the two

5   methods diverge, the observations tend to be related to the thin cloud regimes.

The presence of a multiple solution space in the bispectral LUTs, where small droplet sizes (r_e<5) have the same reflectance as larger droplets, was shown to induce numerous outliers resulting in a significant high bias in the bispectral retrievals for both r_e and (to a lesser extent) τ. This multiple solution space likewise impacts the MODIS operational products, since the bispectral LUTs used in the MODIS collection 6 cloud products include theoretical r_e solutions as low as

10 4 μm. However, for retrievals with multiple LUT solutions the MODIS product only reports the larger r_e value, leading to a systematic bias if the observed cloud really includes a population of small droplets. As a consequence, for thin clouds with small droplet sizes one can expect the comparison of polarimetric and bispectral retrievals to disagree. This strong high-bias for small r_e retrievals provides a plausible explanation for the large discrepancies observed in the small droplet size regime in the intercomparison of MODIS and POLDER retrievals (Bréon and Doutriaux-Boucher, 2005). Absent a solution to this

15 issue, future intercomparisons or combined climatological datasets should be limited to retrievals of r_e(pol) exceeding 5-7 μm (depending on the respective bispectral LUT multiple solution space properties).

At the coarse spatial resolutions of most satellite instruments, cloud inhomogeneity can significantly impact retrievals. In the context of this study we find that the influence of unresolved spatial inhomogeneity is a dominant source of bias between the polarimetric and bispectral r_e retrievals. In this study we found that even for 100% cloudy pixels (at a coarse 800

20 m horizontal resolution) the influence of the PPH bias is significant, with the average r_e bias exceeding 1 μm in the most inhomogeneous LES scene (ATEX clean). Based on these results we expect that the overall systematic bias observed in the MODIS and POLDER intercomparison of moderate droplet size regimes may be attributable to the influence of this PPH bias (Bréon and Doutriaux-Boucher, 2005). Recently, great effort has been made to account for the influence of the PPH bias on bispectral MODIS retrievals. The 2-D Taylor expansion technique implemented by (Zhang et al., 2016) offers the

25 possibility of quantifying (and potentially correcting for) the impact of PPH bias on bispectral retrievals. This approach requires high spatial resolution measurements in at least one spectral band to obtain the sub-pixel reflectance variability, which is used to determine corrections for the bias of r_e and τ. In addition to PPH bias, 3-D radiative effects are also influenced by spatial resolution. The focus on 1-D radiative transfer in this study leaves questions for future studies regarding the influence of these 3-D radiative effects. Future work will need to identify the relative differences between 3-D

30 radiative effects on total and polarized reflectances and retrievals.

Sufficient angular resolution is one of the more important requirements of the polarimetric retrieval technique. We find that resolving the multi-angular polarized reflectance at a resolution coarser than the Nyquist angular resolution of the supernumerary bow results in greater uncertainty (r_e(pol) and v_e(pol)) and biased (v_e(pol)) polarimetric retrievals. The required angular resolution is dependent both on droplet size and wavelength. Future cloud polarimetric instrumentation

should consider these angular resolution requirements. While we have not explicitly tested the so-called "super-pixel" approach implemented for POLDER retrievals, these coarse spatial and angular resolution studies lead to some anticipated biases induced by this technique. We would expect such an approach to further bias v_e(pol) retrievals low, due to the lack of sensitivity to unresolved high-v_e populations. In addition, this current study indicates that r_e(pol) retrieval variance might

5   increase, but the mean bias might not increase significantly. However, if there is significant correlation between the unresolved r_e and v_e populations within an observation footprint, the mean r_e bias would be expected to suffer.

Acknowledgements

    The hardware used in the computational studies is part of the UMBC High Performance Computing Facility (HPCF).

10   The facility is supported by the U.S. National Science Foundation through the MRI program (grant nos. CNS-0821258 and CNS-1228778) and the SCREMS program (grant no. DMS-0821311), with additional substantial support from the University of Maryland, Baltimore County (UMBC). See www.umbc.edu/hpcf for more information on HPCF and the projects using its resources.

Appendix

We often treat the droplet size distribution observed by in-situ instruments (on the order of meters) as relatable to the inferred size distribution properties obtained by remote sensing retrievals (on the order of kilometers). This mathematical analysis addresses how resolution and scale influence the inferred cloud microphysical distribution. The modified gamma-distribution not only suits observations of in-situ cloud droplet size distributions, but it also exhibits several useful mathematical relationships:

$$\langle r^2 \rangle = r_e^2 (v_e - 1)(2v_e - 1)$$
$$\langle r^3 \rangle = r_e^3 (v_e - 1)(2v_e - 1) \qquad . \tag{5}$$
$$\langle r^4 \rangle = r_e^4 (v_e - 1)(2v_e - 1)(v_e + 1)$$

From a retrieval perspective all droplet size distributions are treated as gamma-distributed. There is a potential disconnect here, from the perspective of scale analysis, when retrievals at a 50 m spatial resolution (our LES resolution) and retrievals at 1 km (MODIS retrieval resolution), or even 150 km (POLDER retrieval resolution) each are being treated as gamma-distributed. However, not all droplet microphysics information is created equal; the droplet size distributions at higher resolution (subscript, i) influence the low-resolution (subscript, lr) droplet size distributions. With high-resolution information the different moments of the coarser resolution droplet size distribution should be able to be constructed from the high-resolution microphysics. For a distribution made up of the summation of gamma size distributions the moments of the low-resolution distribution can be expressed by the following relationship, because summation and integration are each linear operators:

$$\langle r^n \rangle_{lr} = \int_r r^n \left[\sum_i^k N_i \left(r, r_{e,i}, v_{e,i} \right) \right] \mathrm{d}r$$
$$\langle r^n \rangle_{lr} = \sum_i^k \left[\int_r r^n N_i \left(r, r_{e,i}, v_{e,i} \right) \mathrm{d}r \right] = \sum_i^k \left[\langle r^n \rangle_i \right] \tag{6}$$

With this mathematical rule in mind, the values of r_e and v_e for the low-resolution droplet size distribution can be obtained by substitution into eq. (2) and eq. (3):

$$r_e' \equiv \frac{\langle r^3 \rangle_{lr}}{\langle r^2 \rangle_{lr}} = \frac{\sum_i^k \langle r^3 \rangle_i}{\sum_i^k \langle r^2 \rangle_i} \quad , \tag{7}$$

$$v'_e \equiv \frac{\langle r^4 \rangle_{lr} \langle r^2 \rangle_{lr}}{\left(\langle r^3 \rangle_{lr}\right)^2} - 1 = \frac{\sum_i^k \langle r^4 \rangle_i \langle r^2 \rangle_i}{\left(\sum_i^k \langle r^3 \rangle_i\right)^{2x}} - 1 \ . \tag{8}$$

Henceforth, we will refer to the r'_e and v'_e relationships in eq. (7) and eq. (8) as microphysical "aggregation rules." It should be noted that these rules fundamentally treat the DSD as gamma-distributed at all scales.

5   The microphysical aggregation rules allow for the explanation of some features of the coarse polarimetric retrieval experiments displayed in Shang et al. (2015). Referring to the inhomogeneous polarimetric retrieval experiments in table 2 and figure 4 of their paper, we reproduced their results and calculated the corresponding r_e' and v_e' in our **Table 2**, which contains the same retrieval examples and corresponding r_e' and v_e' results for the cases examined in their study. There is a clear difference between the mean r_e or v_e and the polarimetric retrieval results. Using the microphysical aggregation rules defined above, we derived that the appropriate distribution properties, r_e' and v_e', are generally in closer agreement with the
10   polarimetric retrievals of r_e(pol). These results offer a possible explanation as to why the polarimetric retrieval does not agree with the average of the sub-scale microphysics in Shang et al.'s study. A couple of things should be noted here: **1)** When there is little variability in the unresolved r_e (e.g., r_e=[15,20] μm) the mean, retrieval, and the estimated mixture are generally all in agreement (e.g., $<r_e>$=17.5, r_e(pol)=18, and r_e'=18.2 μm). **2)** When large variability in the unresolved r_e (e.g., r_e=[5,20]) is present, both the retrieved and estimated mixture strongly favor the larger droplet effective radius (e.g., r_e(pol)=19 and
15   r_e'=19.12 μm). **3)** Large variability in unresolved r_e sometimes results in large differences between v_e(pol) and v_e'. The last two points are likely a consequence of the resulting coarse resolution (multi-modal) distribution differing significantly from the gamma-distribution assumption stated previously.

    Applying this analysis to the aggregation of LES scene microphysics will allow for the determination of how
20   accurate a spatial mean aggregation reflects the true coarse resolution microphysical parameters. We first assumed that all of the highest resolution vertically weighted size-distributions can be assumed to be appropriately characterized by a gamma distribution with r_e=r_e(2WT) and v_e=v_e(2WT). We then aggregated these LES microphysical properties at the 50 m native resolution to increasingly coarser resolutions (100, 200, 400, and 800 m), using both the mean and the aggregation rules. We found that the differences between the two techniques are negligible (Δr_e~0.01 μm and Δv_e~0.001) and do not significantly
25   vary with final resolution. Apparently, the importance of the aggregation rules in the LES are far less important than what we had found in the multiple-moment cases tested in Shang, et al. (2015). One clear difference between the these multiple moment cases and the LES was that the toy models are reductive bimodal distributions, exhibiting very large sub-scale microphysical inhomogeneity in r_e that is not commonly observed in the LES or in observational studies. To address this, we performed a theoretical examination of how important the aggregation rules are for calculating the bias between simple
30   average aggregation and mathematical rule aggregation. In this experiment we established various distributions of

unresolved DSD's with varying r_e and v_e populations. These joint distributions of r_e and v_e were used to test how the variance (i.e., the unresolved variability) would influence the average and mathematical rule aggregated results. This test confirmed, that large differences between the simple average and mathematical aggregation rules requires spatial inhomogeneity of microphysics that much larger than those observed in the LES or typical observational studies. Based on these results we

5   recommend that future studies focusing on the effect of unresolved microphysical inhomogeneity on polarized retrievals should consider more realistic inhomogeneity conditions on both r_e and v_e.

References

Ackerman, A. S., Kirkpatrick, M. P., Stevens, D. E. and Toon, O. B.: The impact of humidity above stratiform clouds on indirect aerosol climate forcing, Nature, 432(7020), 1014–1017, 2004.

Ackerman, A. S., vanZanten, M. C., Stevens, B., Savic-Jovcic, V., Bretherton, C. S., Chlond, A., Golaz, J.-C., Jiang, H.,
5 Khairoutdinov, M., Krueger, S. K., Lewellen, D. C., Lock, A., Moeng, C.-H., Nakamura, K., Petters, M. D., Snider, J. R., Weinbrecht, S. and Zulauf, M.: Large-Eddy Simulations of a Drizzling, Stratocumulus-Topped Marine Boundary Layer, Mon. Wea. Rev., 137(3), 1083–1110, doi:10.1175/2008MWR2582.1, 2009.

Alexandrov, M. D., Cairns, B. and Mishchenko, M. I.: Rainbow Fourier transform, Journal of Quantitative Spectroscopy and Radiative Transfer, 113(18), 2521–2535, doi:10.1016/j.jqsrt.2012.03.025, 2012a.

10 Alexandrov, M. D., Cairns, B., Emde, C., Ackerman, A. S. and van Diedenhoven, B.: Accuracy assessments of cloud droplet size retrievals from polarized reflectance measurements by the research scanning polarimeter

, Remote Sensing of Environment, 125, 92–111, doi:10.1016/j.rse.2012.07.012, 2012b.

Alexandrov, M. D., Cairns, B., Wasilewski, A. P., Ackerman, A. S., McGill, M. J., Yorks, J. E., Hlavka, D. L., Platnick, S. E., Thomas Arnold, G., van Diedenhoven, B., Chowdhary, J., Ottaviani, M. and Knobelspiesse, K. D.: Liquid water cloud
15 properties during the Polarimeter Definition Experiment (PODEX), Remote Sensing of Environment, 169, 20–36, doi:10.1016/j.rse.2015.07.029, 2015.

Bréon, F. M. and Doutriaux-Boucher, M.: A comparison of cloud droplet radii measured from space, IEEE Trans. Geosci. Remote Sensing, 43(8), 1796–1805, doi:10.1109/TGRS.2005.852838, 2005.

Bréon, F. M. and Goloub, P.: Cloud droplet effective radius from spaceborne polarization measurements, Geophys. Res.
20 Lett., 25(11), 1879–1882, 1998.

Cairns, B., Russell, E. E. and Travis, L. D.: Research Scanning Polarimeter: calibration and ground-based measurements, SPIE's Conference on Polarization: Measurement, Analysis, and Remote Sensing II, 186–196, doi:10.1117/12.366329, 1999.

Cho, H. M., Zhang, Z., Meyer, K., Lebsock, M., Platnick, S., Ackerman, A. S., Di Girolamo, L., C Labonnote, L., Cornet, C., Riedi, J. and Holz, R. E.: Frequency and causes of failed MODIS cloud property retrievals for liquid phase clouds over
25 global oceans, J. Geophys. Res., 120(9), 4132–4154, doi:10.1002/2015JD023161, 2015.

De Haan, J. F., Bosma, P. B. and Hovenier, J. W.: The adding method for multiple scattering calculations of polarized light, Astronomy and Astrophysics, 183, 371–391, 1987.

Deirmendjian, D.: Scattering and polarization properties of water clouds and hazes in the visible and infrared, Appl. Opt., 3(2), 187–196, 1964.

30 Deschamps, P. Y., Breon, F. M., Leroy, M., Podaire, A., Bricaud, A., Buriez, J. C. and Seze, G.: The POLDER mission: instrument characteristics and scientific objectives, IEEE Trans. Geosci. Remote Sensing, 32(3), 598–615, doi:10.1109/36.297978, 1994.

Diner, D. J., Xu, F., Garay, M. J., Martonchik, J. V., Rheingans, B. E., Geier, S., Davis, A., Hancock, B. R., Jovanovic, V. M., Bull, M. A., Capraro, K., Chipman, R. A. and McClain, S. C.: The Airborne Multiangle SpectroPolarimetric Imager

(AirMSPI): a new tool for aerosol and cloud remote sensing, Atmos. Meas. Tech., 6(8), 2007–2025, doi:10.5194/amt-6-2007-2013, 2013.

Fridlind, A. M. and Ackerman, A. S.: Estimating the Sensitivity of Radiative Impacts of Shallow, Broken Marine Clouds to Boundary Layer Aerosol Size Distribution Parameter Uncertainties for Evaluation of Satellite Retrieval Requirements, J.
5   Atmos. Oceanic Technol., 28(4), 530–538, doi:10.1175/2010JTECHA1520.1, 2011.

Hansen, J. E.: Circular Polarization of Sunlight Reflected by Clouds, http://dx.doi.org/10.1175/1520-0469(1971)028<1515:CPOSRB>2.0.CO;2, doi:10.1175/1520-0469(1971)028<1515:CPOSRB>2.0.CO;2, 2010.

Hansen, J. E. and Travis, L. D.: Light scattering in planetary atmospheres, Space Sci Rev, 16(4), 527–610, 1974.

King, M. D., Menzel, W. P., Kaufman, Y. J., Tanré, D., Bo-Cai Gao, Platnick, S., Ackerman, S. A., Remer, L. A., Pincus, R.
10   and Hubanks, P. A.: Cloud and aerosol properties, precipitable water, and profiles of temperature and water vapor from MODIS, IEEE Trans. Geosci. Remote Sensing, 41(2), 442–458, doi:10.1109/TGRS.2002.808226, 2003.

Knobelspiesse, K., Segal-Rosenhaimer, M., Redemann, J., Cairns, B. and Alexandrov, M. D.: Multi-angle, polarimetric cloud observations using a radiative transfer model trained neural network, College Park, MD. 2017.

Liu, Y. and Diner, D. J.: Multi-Angle Imager for Aerosols, Public Health Reports, 132(1), 14–17,
15   doi:10.1177/0033354916679983, 2017.

Lohmann, U., Stier, P., Hoose, C., Ferrachat, S., Kloster, S., Roeckner, E. and Zhang, J.: Cloud microphysics and aerosol indirect effects in the global climate model ECHAM5-HAM, Atmos. Chem. Phys., 7(13), 3425–3446, doi:10.5194/acp-7-3425-2007, 2007.

Marbach, T., Phillips, P., Lacan, A. and Schlussel, P.: The 3MI Mission: Multi-Viewing -Channel -Polarisation Imager of
20   the EUMETSAT Polar System - Second Generation (EPS-SG) dedicated to aerosol and cloud monitoring, in Sensors, Systems, and Next-Generation Satellites XVII, vol. 8889, p. 88890I, International Society for Optics and Photonics. 2013.

Martin, G. M., Johnson, D. W. and Spice, A.: The measurement and parameterization of effective radius of droplets in warm stratocumulus clouds, J. Atmos. Sci., 51(13), 1823–1842, 1994.

Martins, J. V., Fernandez-Borda, R., McBride, B., Espinosa, R. and Remer, L.: Combination between in-situ and remote
25   sensing of tropospheric aerosols, College Park, MD. 2017.

Miles, N. L., Verlinde, J. and Clothiaux, E. E.: Cloud Droplet Size Distributions in Low-Level Stratiform Clouds, J. Atmos. Sci., 57(2), 295–311, doi:10.1175/1520-0469(2000)057<0295:CDSDIL>2.0.CO;2, 2000.

Miller, D. J., Zhang, Z., Ackerman, A. S., Platnick, S. and Baum, B. A.: The impact of cloud vertical profile on liquid water path retrieval based on the bispectral method: A theoretical study based on large-eddy simulations of shallow marine
30   boundary layer clouds, J. Geophys. Res., 121(8), 4122–4141, doi:10.1002/2015JD024322, 2016.

Mishchenko, M. I., Cairns, B., Travis, L. D., Kopp, G., Schueler, C. F., Fafaul, B. A., Hooker, R. J., Maring, H. B., Itchkawich, T., Hansen, J. E., Kopp, G., Schueler, C. F., Fafaul, B. A., Hooker, R. J., Maring, H. B. and Itchkawich, T.: Accurate Monitoring of Terrestrial Aerosols and Total Solar Irradiance: Introducing the Glory Mission, http://dx.doi.org/10.1175/BAMS-88-5-677, 88(5), 677–691, doi:10.1175/BAMS-88-5-677, 2007.

35   Nakajima, T. and King, M. D.: Determination of the Optical Thickness and Effective Particle Radius of Clouds from Reflected Solar Radiation Measurements. Part I: Theory, J. Atmos. Sci., 47(15), 1878–1893, doi:10.1175/1520-

0469(1990)047<1878:dotota>2.0.co;2, 1990a.

Nakajima, T. and King, M. D.: Determination of the optical thickness and effective particle radius of clouds from reflected solar radiation measurements. Part I: Theory, J. Atmos. Sci., 47(15), 1878–1893, 1990b.

Planck, M.: The theory of heat radiation, 2nd ed., P. Blakiston's Son & Co., Philadelphia, PA. [online] Available from:
5   http://gutenberg.org/ebooks/40030, 1914.

Platnick, S.: Vertical photon transport in cloud remote sensing problems, J. Geophys. Res., 105(D18), 22919–22935, 2000.

Platnick, S., King, M. D., Ackerman, S. A., Menzel, W. P., Baum, B. A., Riedi, J. C. and Frey, R. A.: The MODIS cloud products: algorithms and examples from terra, IEEE Trans. Geosci. Remote Sensing, 41(2), 459–473, doi:10.1109/TGRS.2002.808301, 2003.

10 Platnick, S., Meyer, K. G., King, M. D., Wind, G., Amarasinghe, N., Marchant, B., Arnold, G. T., Zhang, Z., Hubanks, P. A., Holz, R. E., Yang, P., Ridgway, W. L. and Riedi, J.: The MODIS Cloud Optical and Microphysical Products: Collection 6 Updates and Examples From Terra and Aqua, IEEE Trans. Geosci. Remote Sensing, 55(1), 502–525, doi:10.1109/TGRS.2016.2610522, 2016.

Pruppacher, H. R. and Klett, J. D.: Diffusion Growth and Evaporation of Water Drops and Ice Crystals, in Microphysics of
15 Clouds and Precipitation, pp. 412–463, Springer Netherlands, Dordrecht. 1978.

Roebeling, R. A., Feijt, A. J. and Stammes, P.: Cloud property retrievals for climate monitoring: Implications of differences between Spinning Enhanced Visible and Infrared Imager (SEVIRI) on METEOSAT-8 and Advanced Very High Resolution Radiometer (AVHRR) on NOAA-17, J. Geophys. Res., 111(D20), D20210, doi:10.1029/2005JD006990, 2006.

Rosenfeld, D., Liu, G., Yu, X., Zhu, Y., Dai, J., Xu, X. and Yue, Z.: High-resolution (375 m) cloud microstructure as seen
20 from the NPP/VIIRS satellite imager, Atmos. Chem. Phys., 14(5), 2479–2496, doi:10.5194/acp-14-2479-2014, 2014.

Shang, H., Chen, L., Breon, F. M., Letu, H., Li, S., Wang, Z. and Su, L.: A better understanding of POLDER's cloud droplet size retrieval: impact of cloud horizontal inhomogeneity and directional sampling, Atmos. Meas. Tech. Discuss., 8(7), 6559–6597, doi:10.5194/amtd-8-6559-2015, 2015.

Stevens, B., Ackerman, A. S. and Albrecht, B. A.: Simulations of trade wind cumuli under a strong inversion, J. Atmos. Sci.,
25 58(14), 1870–1891, doi:10.1175/1520-0469(2001)058<1870:sotwcu>2.0.co;2, 2001.

Stevens, B., Lenschow, D. H., Vali, G., Gerber, H., Bandy, A., Blomquist, B., Brenguier, J. L., Bretherton, C. S., Burnet, F., Campos, T., Chai, S., Faloona, I., Friesen, D., Haimov, S., Laursen, K., Lilly, D. K., Loehrer, S. M., Malinowski, S. P., Morley, B., Petters, M. D., Rogers, D. C., Russell, L., Savic-Jovcic, V., Snider, J. R., Straub, D., Szumowski, M. J., Takagi, H., Thornton, D. C., Tschudi, M., Twohy, C., Wetzel, M. and van Zanten, M. C.: Dynamics and chemistry of marine
30 stratocumulus–DYCOMS-II, Bull. Amer. Meteor. Soc., 84(5), 579–593, doi:10.1175/BAMS-84-5-579, 2003.

Stevens, B., Moeng, C.-H., Ackerman, A. S., Bretherton, C. S., Chlond, A., de Roode, S., Edwards, J., Golaz, J.-C., Jiang, H., Khairoutdinov, M., Kirkpatrick, M. P., Lewellen, D. C., Lock, A., Müller, F., Stevens, D. E., Whelan, E. and Zhu, P.: Evaluation of Large-Eddy Simulations via Observations of Nocturnal Marine Stratocumulus, Mon. Wea. Rev., 133(6), 1443–, doi:10.1175/MWR2930.1, 2005.

35 Tampieri, F. and Tomasi, C.: Size distribution models of fog and cloud droplets in terms of the modified gamma function, Tellus, 28(4), 333–347, doi:10.1111/j.2153-3490.1976.tb00682.x, 1976.

Twomey, S.: The Influence of Pollution on the Shortwave Albedo of Clouds, J. Atmos. Sci., 34(7), 1149–1152, doi:10.1175/1520-0469(1977)034<1149:TIOPOT>2.0.CO;2, 1977.

Werner, F., Siebert, H., Pilewskie, P., Schmeissner, T., Shaw, R. A. and Wendisch, M.: New airborne retrieval approach for trade wind cumulus properties under overlying cirrus, J. Geophys. Res., 118(9), 3634–3649, doi:10.1002/jgrd.50334, 2013.

5   Wiscombe, W. J.: Mie scattering calculations: Advances in technique and fast, vector-speed computer codes, NCAR Tech, National Center for Atmospheric Research, Boulder, Colorado. 1979.

Zhang, Z. and Platnick, S.: An assessment of differences between cloud effective particle radius retrievals for marine water clouds from three MODIS spectral bands, J. Geophys. Res., 116(D20), D20215, doi:10.1029/2011JD016216, 2011.

Zhang, Z., Ackerman, A. S., Feingold, G., Platnick, S., Pincus, R. and Xue, H.: Effects of cloud horizontal inhomogeneity
10 and drizzle on remote sensing of cloud droplet effective radius: Case studies based on large-eddy simulations, J. Geophys. Res., 117(D19), n/a–n/a, doi:10.1029/2012JD017655, 2012.

Zhang, Z., Platnick, S., Yang, P., Heidinger, A. K. and Comstock, J. M.: Effects of ice particle size vertical inhomogeneity on the passive remote sensing of ice clouds, J. Geophys. Res., 115(D17), doi:10.1029/2010JD013835, 2010.

Zhang, Z., Werner, F., Cho, H. M. and Wind, G.: A framework based on 2-D Taylor expansion for quantifying the impacts
15 of subpixel reflectance variance and covariance on cloud optical thickness and effective …, Journal of …, doi:10.1063/1.4975502, 2016.

Zinner, T., Wind, G., Platnick, S. and Ackerman, A. S.: Testing remote sensing on artificial observations: impact of drizzle and 3-D cloud structure on effective radius retrievals, Atmos. Chem. Phys., 10(19), 9535–9549, doi:10.5194/acp-10-9535-2010, 2010.

Table 1: Mean values (μ) and standard deviations (σ, in parenthesis) of various optical (τ and H_o) and microphysical properties (r_e(2WT) and v_e(2WT)) of the LES scenes examined in this study. Cloudy pixels is defined using a threshold of $\tau_{LES} > 0.1$.

LES Case	CCN Concentration [#/cm^3]	Scene Cloud Fraction	τ [unitless]	r_e(2WT) [μm]	v_e(2WT) [unitless]	H_o(800 m) [unitless]
DYCOMS-II	60	0.998	17.95 (6.22)	15.52 (1.00)	0.071 (0.11)	0.13 (0.10)
ATEX Clean	40	0.941	7.90 (8.02)	16.93 (2.62)	0.16 (0.12)	0.42 (0.17)
ATEX Poll.	600	0.985	17.48 (14.71)	7.29 (0.91)	0.13 (0.068)	0.24 (0.13)

Table 2: The influence of unresolved microphysical inhomogeneity on polarimetric retrievals is explored in Shang et al. (2015). There results are replicated here and compared to the arithmetic mean r_e ($<r_e>$), and the mathematical aggregation results (r_e' and v_e') defined in eq. (7) and eq. (8).

Sub-scale Size Distribution Mixture		Arithmetic Mean	Polarimetric Retrieval		Aggregation Rules	
r_e	v_e	$<r_e>$	r_e(pol)	v_e(pol)	r_e'	v_e'
[5, 10]	[0.01, 0.01]	7.5	8.0	0.10	9.00	0.060
[5, 15]	[0.01, 0.01]	10.0	14.5	0.01	14.00	0.056
[5, 20]	[0.01, 0.01]	12.5	19.0	0.01	19.12	0.044
[10, 15]	[0.01, 0.01]	12.5	13.0	0.05	13.46	0.040
[10, 20]	[0.01, 0.01]	15.0	16.5	0.10	18.00	0.060
[15, 20]	[0.01, 0.01]	17.5	18.0	0.01	18.20	0.028
[5, 10, 15]	[0.01, 0.01, 0.01]	10.0	12.0	0.10	12.85	0.069
[5, 10, 20]	[0.01, 0.01, 0.01]	11.7	14.0	0.10	17.38	0.087
[5, 15, 20]	[0.01, 0.01, 0.01]	13.3	17.5	0.02	17.69	0.049
[10, 15, 20]	[0.01, 0.01, 0.01]	15.0	16.0	0.10	17.07	0.055
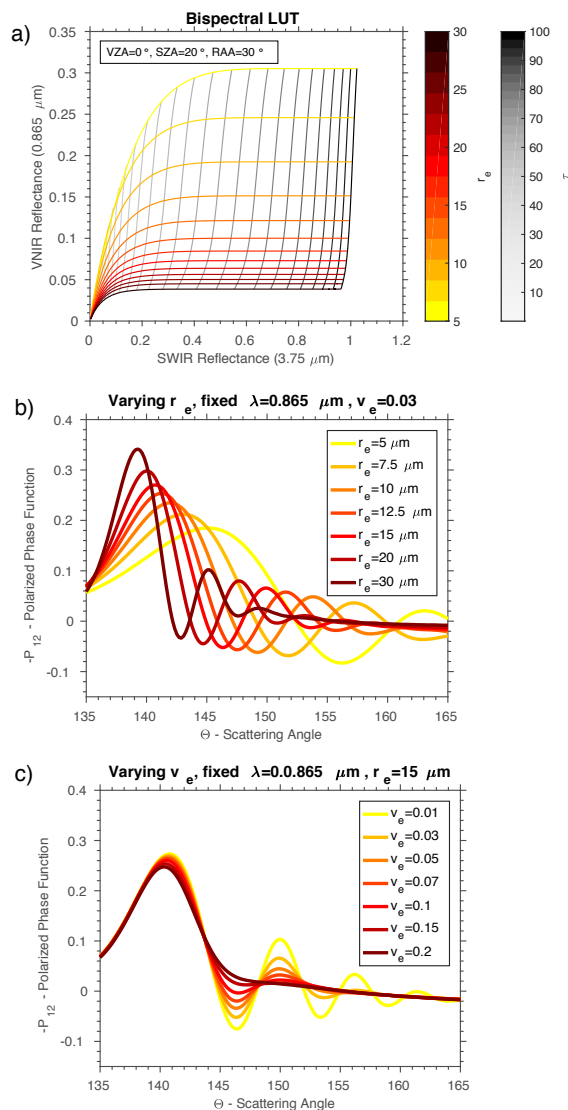
Figure 1: Demonstrations of the microphysical sensitivity of the bispectral and the polarimetric techniques. Panel (a) features the bispectral LUT exhibiting sensitivity to r_e (colored iso-lines), due to absorption in the SWIR reflectance. The VNIR reflectances provide sensitivity to optical thickness (gray iso-lines). Panels (b) and (c) demonstrate the sensitivity of polarimetric technique to r_e and v_e respectively. The supernumerary bow peaks of the polarized phase function ($-P_{12}$) shift and become narrower with increasing droplet size (r_e), whereas the peaks erode in magnitude for broadened droplet size distributions (v_e).
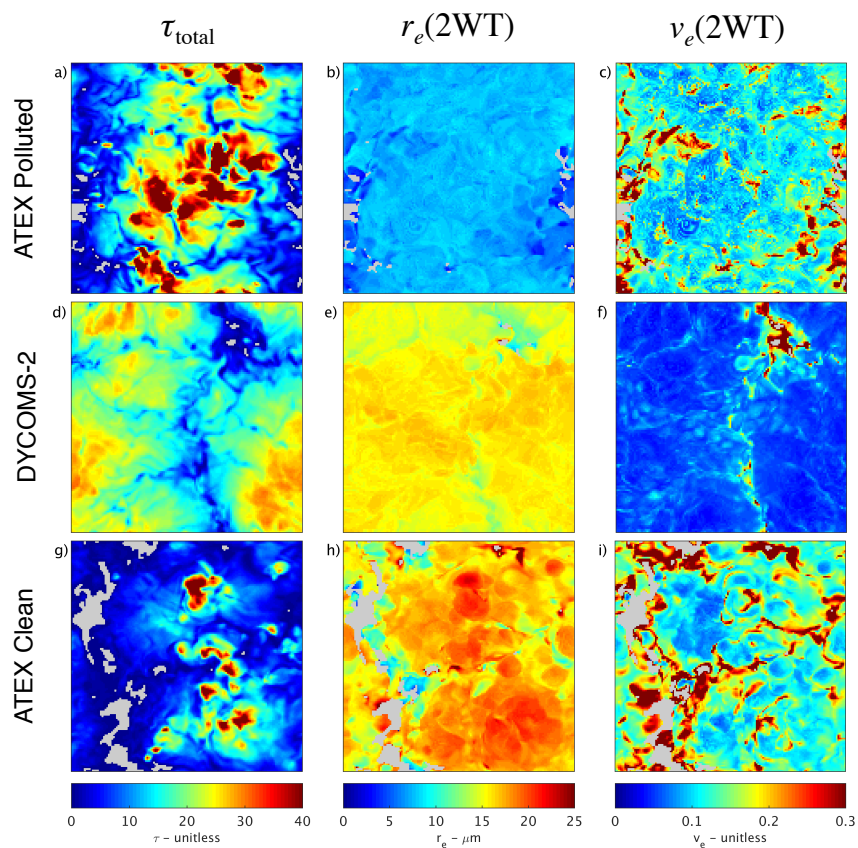
Figure 2: The optical and microphysical properties (τ, r_e, and v_e) of the LES cases examined in this study. The panels are arranged such that each LES case appears row-wise and the different properties are appear column-wise. Cloud-free masking in each of the images appears in gray. Refer to sections 2 and 3 for discussion and definition of each of these properties.

Bispectral Closure Experiment
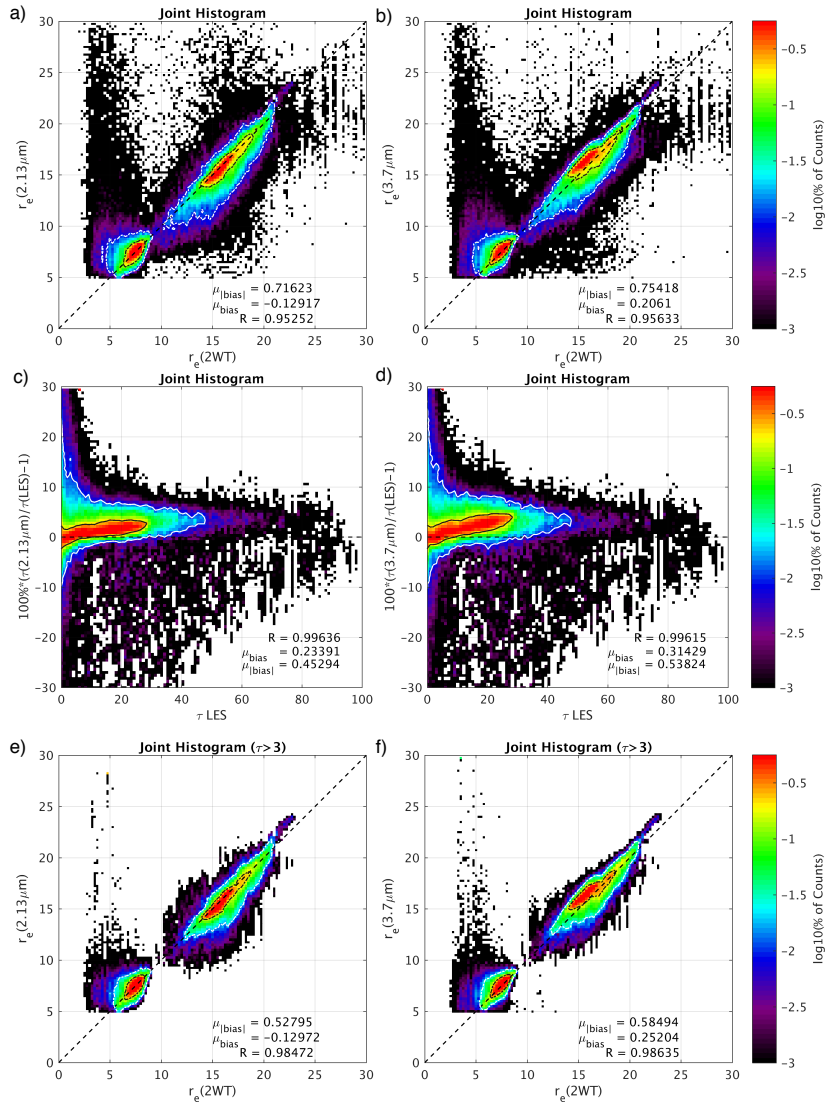
Figure 3: Joint histogram regressions or r_e and τ in all LES cases comparing the bispectral retrievals to the LES cloud microphysical properties. Panels (a) and (b) are regressions of the bispectral r_e(2.13 μm) and r_e(3.75 μm) retrievals against the physical analogue r_e(2WT). Panels (c) and (d) are regressions of the bispectral τ(2.13 μm) and τ(3.75 μm) retrievals against the physical τ(LES). Panels (e) and (f) display the regression of the bispectral r_e(2.13 μm) and r_e(3.75 μm) retrievals for only optically thick pixels (τ>3). Note that in each panel the correlation is quantified with a linear correlation coefficient (R) and the black and white contours encompass 66% and 95% of the population, respectively.
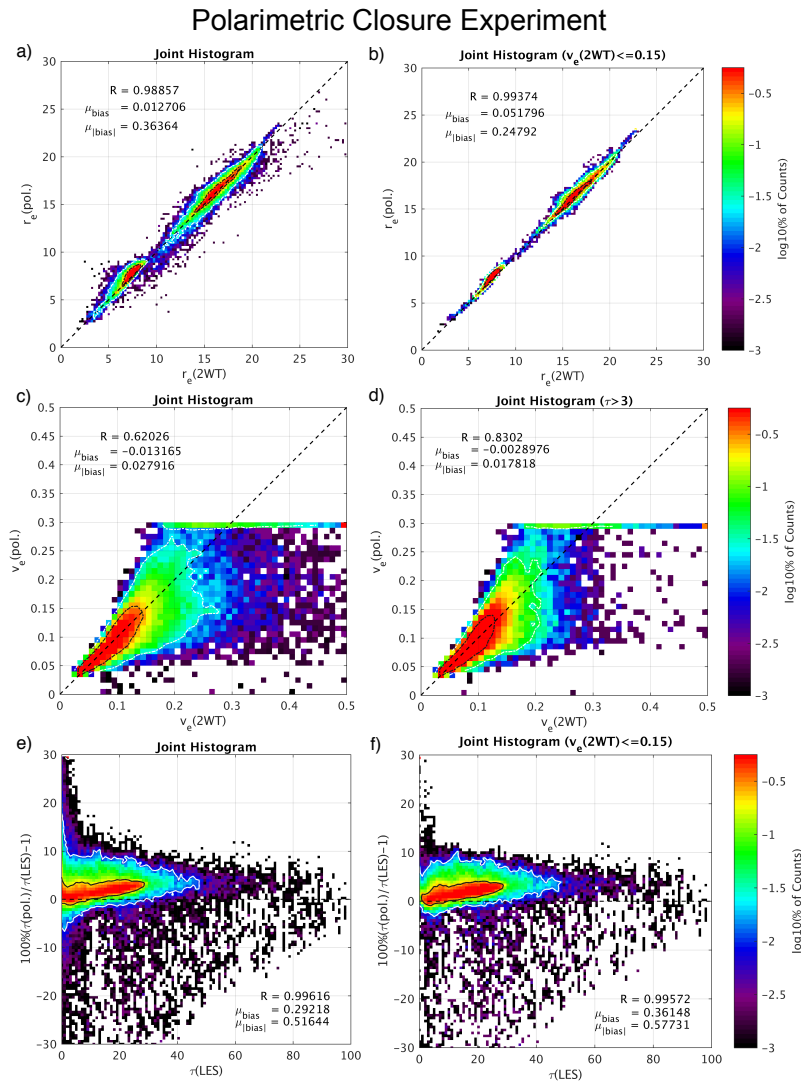
Figure 4: Joint histogram regressions of r_e, v_e, and τ in all LES cases comparing the polarimetric retrievals to the LES cloud microphysical properties. Panel (a) depicts the regression of the polarimetric r_e(pol) retrieval against the physical analogue r_e(2WT), while panel (b) is sub-selection of the same regression for low v_e. Panel (c) depicts the regression of the polarimetric v_e(pol) retrieval against the physical analogue v_e(2WT), while panel (d) is a sub-selection of the same regression for thick clouds ($\tau>3$). Panel (e) depicts the regression of the polarimetric τ(pol) retrieval against the physical analogue τ(LES), while panel (f) is sub-selection of the same regression for low v_e. Note that in each panel the correlation is quantified with a linear correlation coefficient (R) and the black and white contours encompass 66% and 95% of the population, respectively.
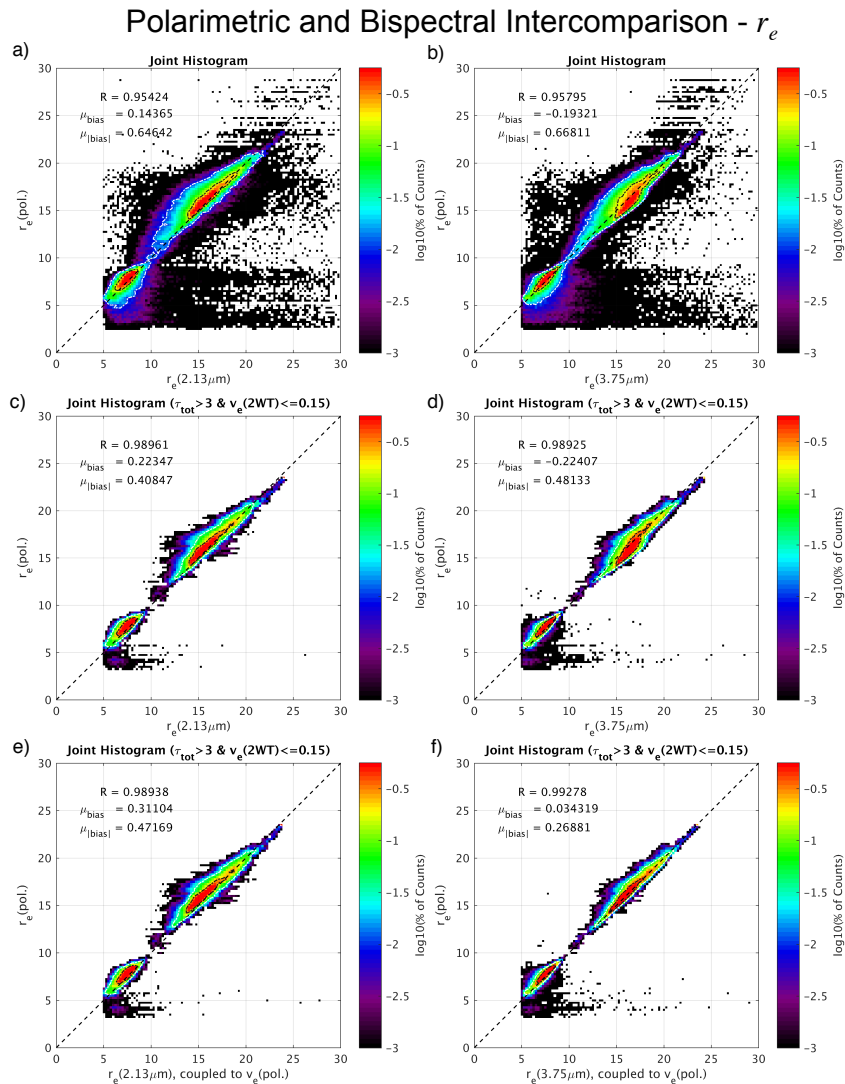
Figure 5: Joint histogram regressions of r_e retrievals for all LES cases comparing the bispectral and polarimetric techniques. Panels (a) and (b) display the unfiltered regressions of r_e(pol) at 0.865 μm wavelength against the r_e(2.13 μm) and r_e(3.75 μm) bispectral retrievals. After introducing filters to these regressions to remove thin clouds (τ<3) and broad droplet size distributions (v_e>0.15) panels (c) and (d) the retrieval intercomparison improves. Panels (e) and (f) each replicate the results from the previous selection criteria but additionally provide bispectral retrieval in this regression with v_e(pol) as an a priori for each retrieval. In each panel the quality of the correlation is quantified and a black iso-contour is drawn surrounding 75% data in the histogram. Note that in each panel the correlation is quantified with a linear correlation coefficient (R) and the black and white contours encompass 66% and 95% of the population, respectively.
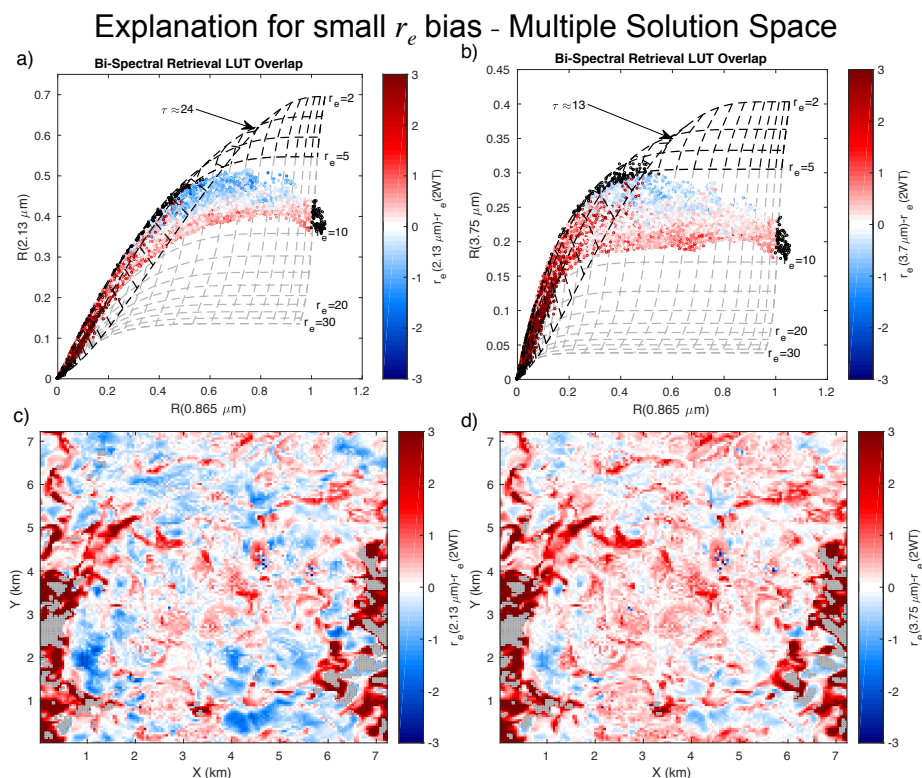
Figure 6: Panel (a) and (b) depict the standard bispectral LUT (light gray dashed lines) for both SWIR bands with the scattered reflectance points for the ATEX polluted LES case plotted overtop. The scatterplot is colored by the bias between the bispectral retrieval and the physical reference (r_e(SWIR)−r_e(2WT)), which is also shown below as a spatial variability map. Note that some reflectance points are colored in black to indicate retrieval failure due to falling outside the standard LUT space. In addition to the standard LUT, an extended LUT including droplet sizes from 2-4μm is included (black dashed lines), revealing an overlapping region of the two LUT for smaller τ referred to as the "multiple solution space".
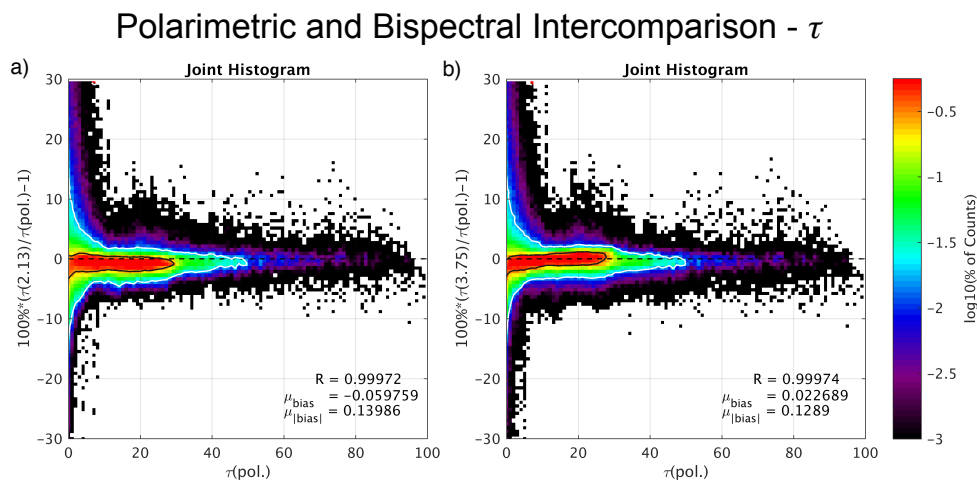
Figure 7: Joint histogram regressions of τ retrievals for all LES cases comparing the bispectral and polarimetric techniques. Panel (a) and (b) display the $\tau(2.13\ \mu m)$ and $\tau(3.75\ \mu m)$ retrievals respectively. In each panel the quality of the correlation is quantified and the black and white population density iso-contours are drawn surrounding 66% and 95% of the data respectively.
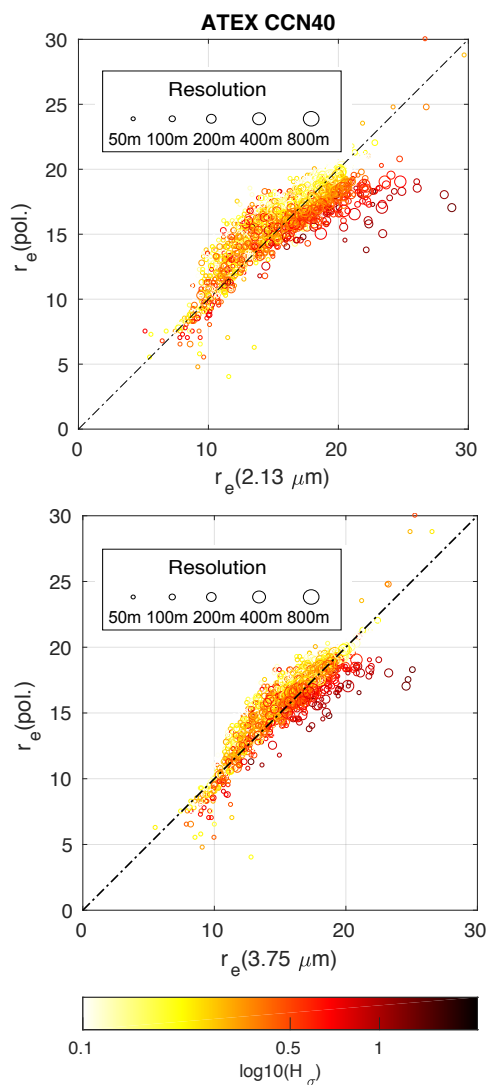
Figure 8: Panel (a) and (b) each respectively compare the r_e(pol) retrieval to the r_e(2.13μm) and r_e(3.75μm) retrievals at increasingly coarsened spatial resolutions (size of circles). The corresponding sub-pixel inhomogeneity (H_σ) of each coarse resolution footprint is also indicated (color of circles).
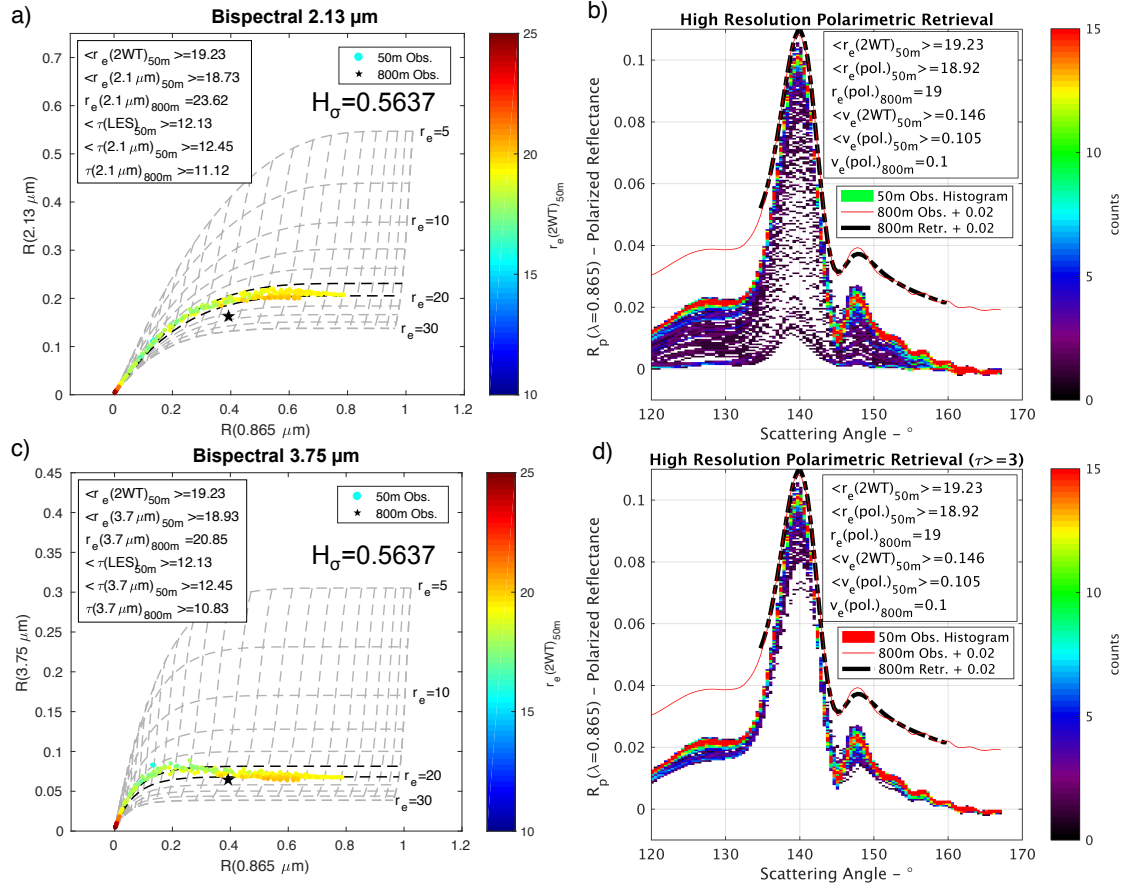
Figure 9: Panels (a) and (c) depict the bispectral LUT's and 50 m reflectances for the 2.13 and 3.75 µm SWIR retrievals respectively for a particularly inhomogeneous 800 m pixel. The scattered points correspond to 50 m reflectances with color corresponding to r_e(2WT), while the black star corresponds to the 800 m reflectance pair (the average of the 50 m data). The polarimetric reflectance distribution histograms in panels (b) and (d) address how the high-resolution (50 m) reflectance distribution influences the polarimetric retrieval at coarse resolution (800m). The two curves (plotted with a 0.02 reflectance shift for clarity) are the 800 m observed reflectance (black dashed curve) and the 800 m retrieval (red solid curve). All of these figures include statistics on the high-resolution averages of physical properties and retrievals along with their coarse resolution counterparts for comparison.
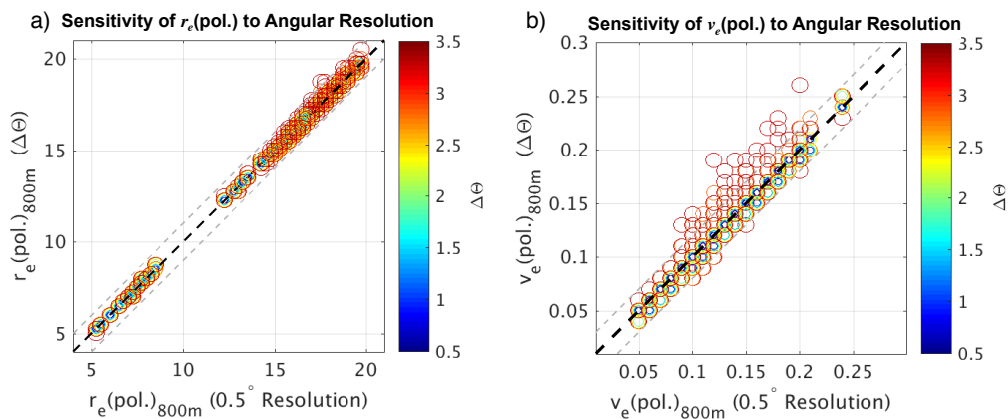
Figure 10: Angular resolution sensitivity experiments examining polarimetric retrievals of r_e (panel a) and v_e (panel b) for all LES scenes at the 800 m spatial resolution. The color and size of scattered points denote the angular resolution of each retrieval. The gray dashed lines denote the ±1 step in the LUT space of the polarimetric retrieval.
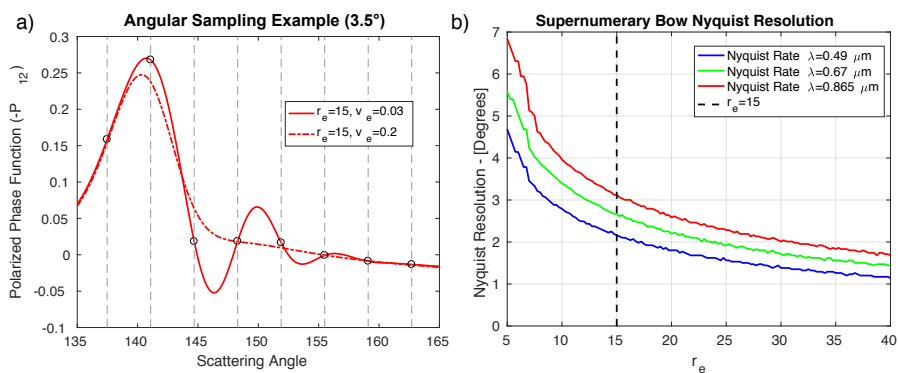
Figure 11: Panel (a) features the polarized phase functions r_e=15 (red) at v_e=0.03 (solid) and v_e=0.2 (dashed). Grey dashed lines and circles indicate a 3.4° observation sampling of the phase functions. The Nyquist resolution is obtained by measuring the peak-to-peak distance of the supernumerary bow oscillations and dividing that distance in half. The Nyquist resolution changes as a function of r_e and λ as shown in panel b, where the gray vertical line highlights the Nyquist resolutions required for the r_e=15 case.